Renewable and Sustainable Energy Reviews 144 (2021) 111037

Contents lists available at ScienceDirect

Renewable and Sustainable Energy Reviews

journal homepage: http://www.elsevier.com/locate/rser

Review of protection systems for multi-terminal high voltage direct current grids

M.J. Perez-Molina *, D.M. Larruskain, P. Eguia Lopez, G. Buigues, V. Valverde

Department of Electrical Engineering, University of the Basque Country UPV/EHU, Plaza Ingeniero Torres Quevedo, 1, Bilbao, Spain

ARTICLE INFO

Keywords:
Algorithms
Fault detection
HVDC transmission
Power system protection

ABSTRACT

Given the current evolution of Voltage Source Converters (VSC), Multi-Terminal High Voltage Direct Current (MTDC) grids are now becoming a real possibility. Still, some technical issues have to be addressed. The protection of High Voltage Direct Current (HVDC) grids is the main technical challenge that is slowing down the development of MTDC grids. Hence, this paper focuses on protection systems. Thus, protection devices, fault-clearing strategies and protection system requirements are considered. The main topic of this paper is the review of different types of protection methods for MTDC systems that are shown in the literature. They can be classified depending on the use of local measurements or a communication channel in their operation. The protection systems reviewed in this paper include protection systems based on current measurements, voltage measurement, traveling wave analysis and artificial intelligence. A protection system can employ only one of these methods or a combination of them. Finally, the main characteristics of the reviewed protection algorithms are compared, highlighting the system configuration, the converter technology, the adopted fault-clearing strategy, the implemented circuit breakers and the size of the limiting inductors. From the work presented in this paper, it is concluded that the actual tendency in MTDC protection systems is predominantly full-selective fault-clearing strategies combined with hybrid HVDC circuit breakers in series with limiting inductors. In addition, most protection methods are based on current measurement algorithms and a considerably high number of the reviewed protection systems employ a combination of several methods benefiting from their combined characteristics.

1. Introduction

Nowadays, High Voltage Direct Current (HVDC) transmission is still a minority versus the traditional High Voltage Alternating Current (HVAC) transmission. Nevertheless, HVDC technology presents some advantages over the traditional HVAC technology (e.g., lower transmission losses and costs over long transmission distances and capability of interconnecting asynchronous grids [1]), which makes HVDC transmission a promising alternative for the electrical system of the future.

However, the characteristics of fault conditions due to the HVDC system's low impedance (i.e., fast increase of the fault current and wide propagation of the voltage drop) make the protection of the HVDC grid quite a challenge. In contrast to Alternating Current (AC) systems, the absence of a "natural" current zero-crossing makes the protection process even more complex. Some of the technical challenges that these HVDC grid protection systems have to faced are:

- The very short protection time available (a few milliseconds), as a result of the vulnerability of the voltage source converters (VSC) to high currents.
- The development of fast and selective protection algorithms.
- The development of fast HVDC circuit breakers capable of creating current zero-crossings, of interrupting high currents and of absorbing high energy.

These technical challenges have to be overcome for the purpose of operating the system efficiently, satisfying the protection requirements.

Several review papers focused on fault detection in HVDC systems have been published over the years. Reference [2] reviews artificial intelligence techniques while the work presented in Ref. [3] reviews fault location techniques. Other works classify the protection methods in unit/non-unit methods [4] or in single-ended/pilot methods [5]. Meanwhile, a selection of different protection methods is reviewed in Refs. [6–8].

However, the work presented in this paper is a complete, extensive

* Corresponding author.
E-mail address: mariajose.perez@ehu.eus (M.J. Perez-Molina).

https://doi.org/10.1016/j.rser.2021.111037
Received 8 July 2020; Received in revised form 2 February 2021; Accepted 23 March 2021
Available online 3 April 2021

List of abbreviations

AC	Alternating current
ANN	Artificial neural network
BU	Backup protection
BiP	Bipole
BB	Busbar protection
CB	Circuit breaker
Com	Communication-based algorithm
CWT	Continuous Wavelet transform
DiffCurr	Differential-current
DC	Direct current
DTFT	Discrete time Fourier transform
DWT	Discrete Wavelet transform
FFT	Fast Fourier transform
FCL	Fault current limiter
FDet	Fault detection method
FIso	Fault isolation method
tiso	Fault isolation time
FLoc	Fault location method
tloc	Fault location time
FCFH	First carrier frequency harmonic
FB-MMC	Full-bridge modular multilevel converter
GPar	Grid partition method
tgpar	Grid partition time
HB-MMC	Half-bridge modular multilevel converter
HIF	High-impedance fault condition
HVAC	High voltage alternating current
HVDC	High voltage direct current
H-CB	Hybrid circuit breaker
LC	Inductor-capacitor
LCL	Inductor-capacitor-inductor
IGBT	Insulated gate bipolar transistor
Loc	Local-measurement-based algorithm
LIF	Low-impedance fault condition
M	Main protection
M − CB	Mechanical circuit breaker
MMC	Modular multilevel converter
MonoP	Monopole
MTDC	Multi-terminal high voltage direct current
OC	Overcurrent
OHL	Overhead line
PtG	Pole-to-ground
PtP	Pole-to-pole
PWM	Pulse-width modulation
ROC	Rate of change
ROCOC	Rate-of-change-of-current
ROCOV	Rate-of-change-of-voltage
SS-CB	Solid-state circuit breaker
S-MonoP	Symmetric-monopole
3L-VSC	Three-level voltage source converter
2L-VSC	Two-level voltage source converter
UV	Undervoltage
VSC	Voltage source converter
WT	Wavelet transform

and up to date review of the different existing fault protection methods for Multi-Terminal High Voltage Direct Current (MTDC) grids, which could be helpful to readers with interests regarding this research field. Therefore, the focus of this paper is fault detection algorithms. Characteristics of HVDC protection devices are overviewed in section 2 and the different topologies of circuit breakers are presented. Fault-clearing strategies and protection requirements are described in sections 3 and 4, respectively. Afterwards, local-measurement-based and communication-based methods are reviewed in section 5. Thereafter, a comparison of the reviewed protection methods is presented in section 6. Finally, some conclusions of this work are detailed.

2. Protection devices

Fault current interruption is more complex in HVDC systems because of the absence of a "natural" current zero-crossing [9,10]. In addition, the fault current rises to very high values and it spreads to the entire system in a range of time of just a few milliseconds, as a result of the HVDC grid's low impedance [11]. This situation worsens when modern VSC converters are employed, since their insulated gate bipolar transistors (IGBT) are vulnerable to high currents [12] and can only withstand twice the rated current [13,14].

Traditionally, circuit breakers (CB) placed on the AC side of the system protected point-to-point HVDC systems employing current source converters. The operation speed of AC-CBs take several cycles, in the order of tens of milliseconds [15], due to mechanical restrictions. Moreover, after a trip the entire link is shut down. Likewise, AC-CBs are not appropriate for MTDCs since a shutdown of the entire grid is not feasible [16].

Therefore, fast and reliable HVDC-CBs are needed for selective fault isolation in a MTDC, ensuring that the unaffected parts of the system keep their operation [17]. Hence, they have to fulfil a series of requirements [12]:

- Capability of creating a current zero-crossing, allowing fault current interruption [18].
- Fast operation in the order of a few milliseconds [19].
- Capability of interrupting the high fault-induced currents [20].
- Minimum power losses and cost for efficient operation of the system [21].
- Capability of energy dissipation in order to prevent overvoltages derived from the current interruption process [22].

Different types of HVDC-CBs and current interruption methods have been developed over the last few years in order to fulfil these requirements. Mechanical HVDC-CBs are mostly based on available AC devices and auxiliary components which interrupt the fault current by injecting a reverse current or by generating a counter voltage. Solid-state HVDC-CBs employ semiconductor devices to interrupt the fault current. Hybrid HVDC-CBs combine the main characteristics of the two previous CBs, obtaining an advantageous operation.

2.1. Mechanical HVDC-CB

Mechanical HVDC-CBs (M − CB) are based on the operation of conventional AC-CBs by using common AC interrupters (vacuum-based, SF6-based, air-blast-based, etc.) and an auxiliary branch. This additional branch generates a current zero-crossing on the interrupter, basically, by reverse-current-injection or by counter-voltage methods, extinguishing the arc and allowing the complete opening of the CB. This CB technology uses conventional and available components which lowers the costs [23]. However, since it depends on AC interrupters, its operation is too slow, limited to several tens of milliseconds. On the other hand, M-CBs present low on-state losses. In addition, the generation of the current zero-crossing adds complexity to the M − CB in comparison to AC-CB technology [11]. Furthermore, an energy absorber path consisting in surge arrester banks (commonly metal oxide arresters) dissipates the energy stored in the system inductance, since it is technically more

appropriate to absorb the energy in this additional device than in the electric arc produced by the opening of the interrupter [24].

The interrupter is a key component of HVDC-CBs. Its contacts have to be able to create a distance that ensures an adequate dielectric strength. Moreover, their operation speed affects the time needed for arc extinction [25] and the total breaking speed of the CB [26]. Vacuum interrupters present advantageous characteristics, such as the small gap required to achieve full dielectric integrity and circuit isolation, and the relatively low mass inertia of the moving system [27]. They are mostly used due to their excellent insulating properties after a current zero [28].

The current zero-crossing is generated by producing a counter voltage or by injecting an opposing current to the fault current. Basically, the counter-voltage method consists on generating the arc voltage by opening the switching device, which is opposed in excess to the voltage of the system, driving the current to zero. The voltage through the CB has to exceed the system voltage until the current reaches zero, simultaneously dissipating the magnetic energy stored in the grid inductance [29]. This voltage level must be in the range of 1.2 and 1.5 of the rated voltage [30,31].

Meanwhile, the reverse-current-injection method consists in producing a current zero-crossing by an auxiliary circuit, commonly an inductor-capacitor (LC) resonant circuit where the pre-charged capacitor discharges in opposition to the fault current, extinguishing the arc and completing the opening of the switch. The reverse-current-injection magnitude must exceed the fault current and the initial charge of the commutation capacitor must provide a safety margin to interrupt the largest expected current [32]. This method can be based on passive- or active-resonance. In the passive-resonance method, the resonant LC circuit is self-excited or naturally trigged by the arc generated in the opening of the AC interrupter, due to its negative resistance and natural fluctuations [33]. On the other hand, in the active-resonance method, the capacitor of the LC circuit is pre-charged and it is inserted in the circuit by a switch [34], enabling a faster current interruption [18] since there is no time delay due to the generation of the oscillating current [33]. However, a charging unit is needed, which increases the costs [35]. Fig. 1 shows the basic topologies of a counter-voltage-based, a passive–resonance-based and an active-resonance-based M-CB.

The VSC assisted resonant current (VARC) CB is a modern model of M-CB. This topology presents a vacuum interrupter actuated by an ultra-fast Thomson-coil mechanism in the main branch. A VSC is introduced in series with the LC resonant circuit in the auxiliary branch to generate a frequency oscillating current. This way, a current zero-crossing is created when the amplitude of the oscillating current reaches the amplitude of the fault current and the current is extinguished in the energy absorber branch [36]. A prototype with a maximum current interruption capability of 10 kA and a transient interruption voltage of 40 kV was developed within the frame of the PROMOTioN project [37]. This topology is represented in Fig. 2-a.

2.2. Solid-state HVDC-CB

Solid-State HVDC-CBs (SS-CB) consist on semiconductor components, mostly fully-controlled devices [38]. They present the fastest operation time, in the order of several microseconds [12,20], due to the almost instantaneous operation of the semiconductors. This technology is fast enough to avoid damaging levels of the fault current [39], hence it operates with a reduced maximum current due to its operation speed [40]. However, a large number of semiconductors are needed for high voltage applications, which increases the cost of this topology. In addition, these devices present a high on-state voltage drop and, consequently, high on-state losses. A semiconductor with a few kV of voltage rating presents an on-state voltage drop in the range of a few volts, generating losses in the range of kW for a current in the order of hundreds of amperes [29]. These losses can be in the range of 0.1–0.4% of the transmitted power [19] or up to 30% of a VSC converter's power losses [12]. Besides, they also present some problems related to asynchronous operation and voltage and current balancing [41].

A basic scheme of a SS-CB is depicted in Fig. 2-b and it presents two branches: a main conduction branch with the main breaker, which is a series connection of several semiconductor devices (commonly IGBTs), and an energy absorber branch with surge arrester banks, usually metal oxide arresters. The current is conducted through the IGBTs during normal operation. The semiconductor devices are turned off after fault detection, commutating the current to the energy absorber branch, where it is driven to zero since the arrester voltage exceeds the system voltage. Finally, the system energy is dissipated.

2.3. Hybrid HVDC-CB

Hybrid HVDC-CBs (H-CB) combine the advantageous characteristics of M − CB and SS-CB into its topology by mixing mechanical interrupters and semiconductor devices [42]. This way, a fast operation is achieved with lower on-state losses. However, H-CB still presents a relatively high cost as a result of the use of several semiconductor components and the complexity of its structure [23].

Fig. 3 shows a basic H-CBs topology consisting of three branches: the main branch, which consists of a fast mechanical switch and a semiconductor-based load commutation switch; the auxiliary branch, formed by a main semiconductor-based breaker; and the energy absorber branch, composed of surge arrester banks. The main breaker does not contribute to the on-state losses since it only conducts current for a brief period during the current interruption process. Hence, power losses in the main branch are mostly caused by the few semiconductor devices that constitute the load commutation switch [13]. Likewise, the main breaker does not need a forced cooling system since the current

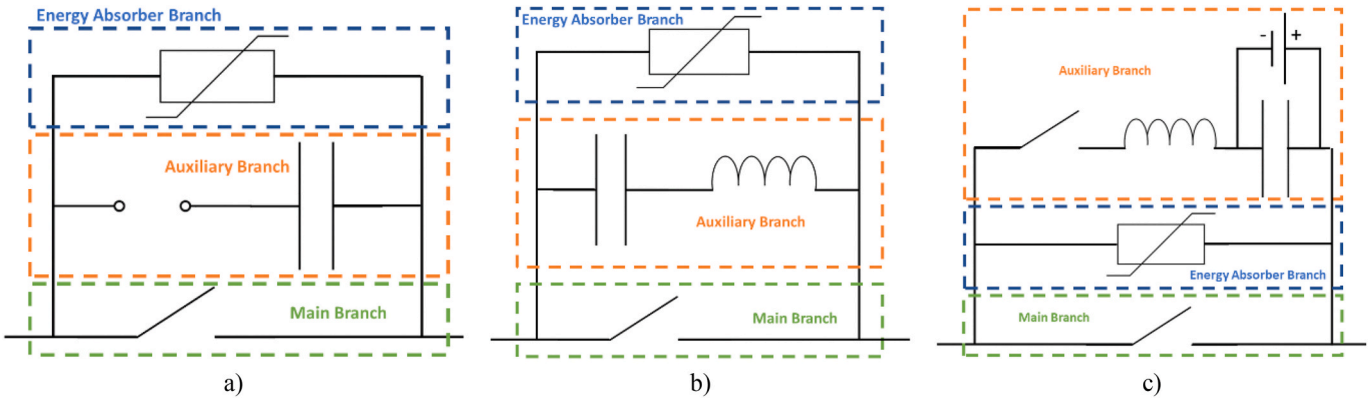

Fig. 1. M-CBs based on a) counter-voltage method, b) passive-resonance method, c) active-resonance method.

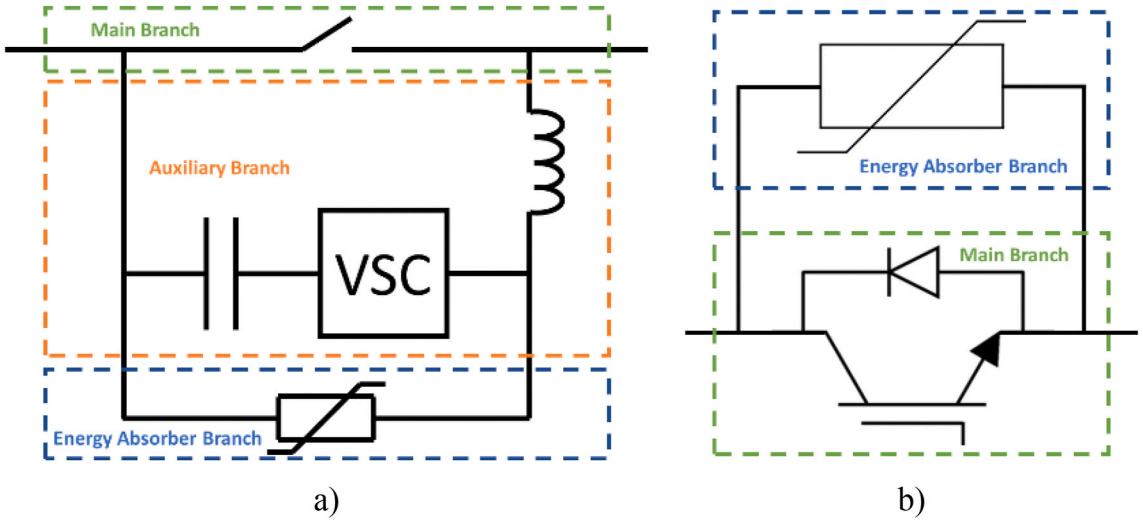

Fig. 2. Basic topologies of a) VARC-based M − CB, and b) SS-CB.

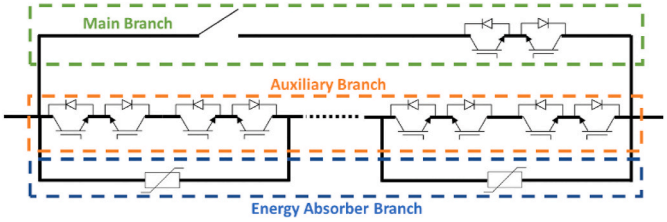

Fig. 3. Topology of a H-CB.

does not flow through it for a long time, although this cooling system is required by the load commutation switch [43].

After fault detection, the main breaker turns on and the load commutation switch turns off, forcing the current to the auxiliary branch. This way, the fast mechanical switch begins separating its contacts under a zero current condition with low stress. Hence, a fast mechanical disconnector with a lightweight contact system can be employed in this type of CB [23]. In addition, the main limitation of the interruption time of the breaking device is the fast mechanical disconnector's opening speed [44], since the operation time of the semiconductor devices is almost instantaneous. Finally, when the mechanical switch is completely opened, the main breaker is turned off, commutating the current to the energy absorber branch where it is driven to zero while absorbing the system energy [45].

2.4. Developed HVDC circuit breakers

Table 1 presents the characteristics of different HVDC-CBs which have been developed by different manufacturers or which are installed (or planned to be installed) in existing MTDCs.

Table 1
Characteristics of manufactured/installed circuit breakers.

Manufacturer/ MTDC	Technology	Rated Voltage	Breaking Capability	Operation Time
ABB [46]	Hybrid	320 kV	9 kA	2 ms
Alstom [30]	Hybrid	120 kV	7.5 kA	2 ms
SCiBreak AB [36, 37]	VARC-based Mechanical	40 kV	10 kA	3 ms
Nan'ao MTDC [47]	Mechanical	160 kV	9.2 kA	3.9 ms
Zhoushan MTDC [48]	Hybrid	200 kV	15 kA	3 ms
Zhangbei MTDC [49]	Hybrid	500 kV	25 kA	3 ms

3. Fault-clearing strategies

Fault-clearing strategies determine the impact of a fault condition on a grid. They depend on the protection equipment implemented in the system [50], as well as on the main objective of the protection system, which can be the stability of the HVDC side or of the AC side of the grid. The fault-clearing time is restricted and constrained to a few milliseconds before any VSC converter blocks when the focus is on the HVDC side's stability. This way, the disturbances and effects caused by the fault condition are minimized. On the other hand, when the main priority is the AC side's stability, the fault-clearing time can be longer and it is only restricted by the AC system constraints. This way, converter blocking is allowed and a large zone of the HVDC system or even the entire HVDC system can be affected and shut down.

In this regard, there are three possible strategies: non-selective, full-selective and partially-selective.

3.1. Non-selective fault-clearing strategy

In this strategy, AC-CBs shut down the entire system after fault detection. Afterwards, direct current (DC) disconnectors, placed at the ends of each link, isolate the faulty part. Finally, AC-CBs are re-closed and the system is re-energised. This kind of strategy is usually selected with fault tolerant converters [4].

3.2. Full-selective fault-clearing strategy

This strategy considers that each link and relevant component of the HVDC grid constitutes a protection zone, so HVDC-CBs are situated at the limits of all protection zones. Only the affected zone of the system is disconnected. This strategy tries to resemble the conventional AC protection strategy.

3.3. Partially-selective fault-clearing strategy

This strategy combines the full-selective and the non-selective strategies. The grid is split into different protection subsystems, attached by links where DC/DC converters or HVDC-CBs are located. The subsystems are disconnected from each other when fault detection is achieved. Then, AC-CBs shut down the affected subsystem, including its healthy parts, and DC disconnectors isolate the affected part. Finally, the healthy

parts are reenergised.

4. Protection requirements

Fault conditions have to be isolated as fast as possible due to their damaging characteristics [8]. The fault effects on the healthy zones of the system must be minimized, avoiding damages on components. Thus, the isolated part of the grid should be as small as possible [51]. Besides, if a large part of the HVDC system is shut down, the AC grid stability could be affected. Hence, the protection must minimize the fault's impact and ensure the systems' safety [15,52]. To achieve all this, a HVDC protection system must fulfil some performance requirements [53,54]:

- Accuracy: operation against internal fault conditions.
- Speed: fast fault detection, identification and clearance, in less than 10 ms [55,56].
- Sensitivity: detection of every relevant fault condition.
- Selectivity: proper discrimination between internal and external fault conditions, so only the affected zone is isolated.
- Seamlessness: reaching a stable operation after fault clearance [57].

5. HVDC protection methods

Protection methods can be classified according to the procedure used to take the measurements needed for their operation. Local-measurement-based protection systems use only locally available measurements for fault detection [4,52] while communication-based protection systems are characterised by the exchange of information between the ends of the protection zone [4,52].

Local-measurement-based protection systems usually discriminate faults by monitoring and measuring DC current and voltage waveforms. These measurements can be used directly in overcurrent and undervoltage algorithms, or they can be mathematically processed calculating their rate of rise or extracting their most interesting and useful features. This type of protection method presents a very fast operation since it only takes single-ended measurements into account, but it is challenging in terms of selectivity [53,58]. Some examples of this kind of methods are: undervoltage, rate-of-change-of-voltage, overcurrent and rate-of-change-of-current.

Inductors are usually placed at both ends of each link when a local-measurement-based algorithm is selected. This component is relevant since it improves the selectivity of the protection method. The inductors damp external signals and, this way, delimit the borders of the protection zones. Furthermore, limiting inductors can limit the increase of the fault current, thus, allowing the implementation of circuit breakers with lower current interruption capability. Nevertheless, their size can affect the system stability [46]. Their size is chosen depending on the selected algorithm and the characteristics of the protected grid.

Conversely, the fault discrimination threshold affects the performance of a local-measurement-based algorithm. This threshold affects the selectivity and sensitivity of the protection algorithm, and it depends on the characteristics of the grid, so it must be selected through simulations [59]. A higher value upgrades the system's selectivity but downgrades its sensitivity.

Communication-based protection methods are inherently selective but they present limitations in terms of speed as a result of the time delay imposed by the communication channel [4,54,55]. Hence, the most critical parameter for the protection operation is the communication time delay [52,60]. Besides, the protection system could reach a non-operative state if there is a problem in the communication channel [4], consequently, they are not regarded as a very reliable method. This way, communication-based methods are not appropriate for long transmission distances [4,6,52,61]. Furthermore, this kind of method is mostly used in conditions of high-impedance faults since the requirements of speed are not very critical [62] and as a backup protection to improve the main protection performance [52,63]. Among the most common communication-based methods, differential-current and directional-current can be mentioned.

Other types of protection methods are those based on detecting the traveling wave generated by a fault condition and those using artificial intelligence techniques to detect and locate the fault conditions. These methods can be either local-measurement-based or communication-based. Traveling-wave-based protections employ mathematical transforms to extract the frequency content of the traveling wave, e.g., Wavelet transform [64,65] and Fourier Transform [66,67]. They use the frequency features to discriminate between fault conditions and normal operation. Nevertheless, the artificial-intelligence-based approach uses computation to resemble the process made by human beings during decision making. Artificial neural networks [68,69] are an example of artificial intelligence techniques.

5.1. Current-based protection methods

Protection systems based on algorithms using features of the DC current signal are reviewed in this section.

5.1.1. Overcurrent algorithm

A basic current-based method is the overcurrent (OC) algorithm [4]. The DC current is locally monitored and compared with a pre-defined threshold. Fault detection is achieved when the threshold is exceeded [55]. Directionality can be achieved by monitoring the current polarity [52]. It presents fast operation but it lacks selectivity [53,58]. However, it can be used as a robust backup protection method [52].

An OC protection for a radial VSC-MTDC system is proposed in Ref. [70]. The current magnitude is compared with an OC threshold of 2.1 p.u. for fault detection. Another OC protection method is used in Ref. [71] in order to protect a 4-terminal symmetric-monopole MTDC system. Another OC method is proposed for fault detection in a 3-terminal MTDC system in Ref. [72]. Likewise, paper [58] proposes an inverse time overcurrent method which protects a 3-terminal bipole MTDC system; the higher the current is, the faster the operation will be.

Authors of [73] propose a coordination method for overcurrent relays based on communication between the relays. A reduced number of H-CBs are used to reduce costs, so they are placed on the active elements' connection points. The CBs operate after fault detection by instantaneous overcurrent relays. Afterwards, the OC relays exchange operation information to locate the fault allowing switches to isolate the faulty part and, then, the CBs are reclosed.

In [74], HVDC-CBs divide a 5-terminal VSC-HVDC grid into two protection zones. These devices are located in the DC link that interconnects both zones. Thus, when a fault is detected by an OC algorithm, the HVDC-CBs operate and disconnect the protection zones, allowing the healthy zone to remain operative. Finally, the AC-CBs of the faulty zone are triggered. A similar protection strategy is presented in Ref. [75]. Apart from the protection zone division by HVDC-CBs, an alternative using DC/DC converters is proposed. Fault detection is achieved when the arm current of the DC/DC converters exceeds its internal overcurrent threshold, and the converters are blocked disconnecting the zones. Same authors of [75] use the DC/DC converter alternative as protection strategy for a 6-terminal MTDC grid in Ref. [76].

An analysis of the OC method is presented in Ref. [77] for a 4-terminal symmetric-monopole modular multilevel converter (MMC) system. H-CBs and 150 mH limiting inductors are employed, adopting a full-selective strategy. The OC performance is tested against different fault conditions. This way, the OC algorithm presents an operation time in the range of 1–7 ms, depending on the fault distance. In addition, it presents better performance against Pole-to-pole (PtP) fault conditions than against Pole-to-ground (PtG) fault conditions, in the case of high-impedance faults.

Reference [78] proposes a combination of the OC algorithm with a

multiple decision criteria in a 4-terminal bipole MMC-MTDC. SS-CBs are employed for current interruption while no limiting inductors are placed in the system. The multiple decision criteria is based on an undervoltage algorithm, detecting first a negative current and a subsequently positive current within a determined time range, and a current-derivative algorithm. This way, the selectivity and sensitivity of the protection scheme are improved. Fault conditions with impedances of 0.5 Ω and 20 Ω are cleared in 8.74 ms and 11.26 ms, respectively.

5.1.2. Rate-of-change-of-current algorithm

The rate-of-change-of-current (ROCOC) algorithm consists in measuring the DC current and calculating its derivative as in (1):

$$ROCOC = \frac{\Delta I}{\Delta t} = \frac{I_2 - I_1}{t_2 - t_1} \tag{1}$$

where I_1 is the magnitude of the DC current at a certain time t_1 and I_2 is the magnitude of the DC current at a certain time t_2, being time t_2 higher than time t_1.

Ideally, the value of this derivative should be zero during normal operation conditions and increase during fault conditions. However, the reality is that the derivative is not zero during normal operation due to fluctuations and disturbances. Then, the current-derivative is compared with a pre-defined threshold, ensuring selectivity [52,55,79]. In other cases, the polarity of the first peak of the ROCOC is used as a fault marker: a positive polarity indicates a forward fault; otherwise it is a backward fault [55,80]. However, this last method might lead to unnecessary and erroneous trips due to oscillations in the signal; measurements taken right after a local minimum/maximum of the current signal will indicate a forward/backward fault regardless of the actual fault location [79]. This method allows a faster fault detection than the OC algorithm [81]. However, the ROCOC of a remote high-impedance fault can be lower than the ROCOC of an external fault [4].

In this regard [82], presents a protection system based on ROCOC. It is concluded, through simulations and experimental studies, that this method presents reliable and fast operation. An analysis of the applicability of a communication-based algorithm to a 5-terminal MTDC system is presented in Ref. [61]. This algorithm compares the current-derivative sign at both ends of a link. A fault is detected when these two derivatives present the same sign. The authors assert that the applicability of a communication-based algorithm in this system is challenging, since the critical fault-clearing times cannot be satisfied because of the imposed communication time delay. A protection system consisting on a ROCOC algorithm protects a 3-terminal bipole MTDC grid in Ref. [80]. The DC current is measured locally, its derivative is calculated and then its first peak is analysed. A forward fault is detected if this peak shows a positive polarity. If the peak is negative, the fault is located in the backward direction. 10 mH Fault Current Limiters (FCLs) are placed in series with HVDC-CBs at both ends of each link so as to enhance the selectivity. The protection operation time is lower than 3 ms. Reference [83] presents a protection scheme for a 3-terminal bipole MTDC system against faults with different impedances. Inductive FCLs are employed to ensure selectivity while limiting the increase of the current. The DC current-derivative is compared with a threshold of 1.5 kA/ms. The polarity of the current is monitored to add directional selectivity. Furthermore, an overcurrent condition has to be fulfilled in order to trip the CBs. Similarly, a rate-of-change-of-voltage algorithm is applied to the MTDC system presented in Ref. [77]. A discrimination threshold of 3 kA/ms and limiting inductors with a size of 100 mH are employed in this case. This method presents a detection time around 1 ms, depending on the fault distance. However, its application to detect high-impedance faults might be challenging.

Reference [84] presents a fault location algorithm consisting of the Rate Of Change (ROC) of the discharging current of the converter filter capacitor. It can be employed to detect both high- and low-impedance faults, since the initial ROC is very similar for both cases and is mostly dependent on the fault location. However, this method is still challenging because the ROC decays exponentially over time, so a delay in the measurements might mean a non-accurate location of the fault, mistaking it as an external fault. Reference [85] proposes a fault detection algorithm based on calculating the correlation-coefficient between the ROC of the DC line current and the ROC of the discharging current of the DC link capacitor. This way, the correlation-coefficient is calculated when the ROC of the line current surpasses a certain threshold. Fault detection is achieved when this coefficient is close to the unity. This method shows a detection time lower than 1 ms, which it is not influenced by the fault location.

An algorithm consisting on calculating the derivative of the differential-current of each pole is proposed in Ref. [86] for fault type discrimination and fault detection. The input and output currents of a pole are summed, afterwards derived and finally compared with a threshold. This method adds speed to the conventional differential-current method.

A faulty conductor identification algorithm based on the ROCOC is presented in Ref. [81] for a 3-terminal bipole VSC-HVDC system. This algorithm allows to distinguish PtG faults, PtP faults and faults involving the dedicated metallic return conductor. The fault marker is the ratio between the maximum ROCOC of two conductors. The fault type is identified by comparing the value of this ratio, for different pairs of conductors, with their respective thresholds.

5.1.3. Differential-current algorithm

Differential-current algorithms consist of summing the input and output currents of a link or busbar [52,55]. They reflect that the current flowing in and out of a protection zone is not the same in the case of a fault condition.

The differential-current on a busbar is calculated in (2):

$$\mathrm{DiffCurr_{bus}} = \sum_{i=1}^{n} \mathrm{I_i} \tag{2}$$

where I_i is the current flowing through each line connected to the busbar and n is the number of lines connected to the busbar.

The differential-current on a link L_{ij} is calculated in (3):

$$\mathrm{DiffCurr_{line}} = \mathrm{I_{ij}} + \mathrm{I_{ji}} \tag{3}$$

where I_{ij} is the current measured at one end of the link and I_{ij} is the current measured at the other end of the link.

This differential-current is a vector sum in the case of HVAC systems, while it is an algebraic sum in HVDC systems and it is calculated individually in each pole.

If the value of the differential-current is higher than a threshold, a tripping signal is issued to the corresponding CBs [8]. By comparing this value to a threshold, possible oscillations due to normal operation changes are not mistaken as a fault. Then, this algorithm is a very robust and selective method [54], which also provides directionality [4], allowing the isolation of the affected part of the system while the healthy parts remain operating unaffected. However, in the case of line protection, the operation speed of this algorithm is challenging since it is restricted by the communication time delay [6,52,55], which depends on the medium of the communication channel and on the cable length. This parameter is the most critical, since even with an optic fibre channel (delay of 0.5 ms per 100 km [6,56,61,87]), its operation might not be fast enough [60]. This algorithm is only used as main protection for short transmission distances [61]; hence, it is mostly used as a backup protection to improve the protection performance [63] and in high-impedance fault [62].

A differential-current algorithm is proposed in Ref. [56] as the main protection of a 5-terminal bipole VSC-HVDC grid. An optic fibre channel is employed in the communication channel. This algorithm requires that three consecutive samples fulfil the detection condition in order to

produce the tripping signal. This way, the probability of misdetection is considerably reduced. The protection system operates properly in cases of high-impedance faults, up to 200 Ω. The same protection system and grid are used in Ref. [88], but resistive superconducting FCLs are employed, limiting the increase of the DC current and helping the CBs to interrupt lower values of current. Likewise [89], uses the same protection system and MTDC grid presented in Refs. [56,88]. The differential-current-based protection system proposed in Ref. [90] covers main, busbar and backup protections of a 5-terminal bipole MTDC system. Fibre optic is used as communication channel medium. As in Refs. [56,88], the main protection needs three consecutive samples to generate the tripping signal. In the case of the busbar protection, all the currents flowing in and out the busbar through the branches are summed to detect faults located between the converter station and the relays located at the beginning of every link. The backup protection aims to operate in cases of failure of the main protection by tripping all the CBs located in the closest busbar; its operation starts after a certain time delay. The same protection system proposed in Ref. [90] is used again in Ref. [87] but, in this case, a 4-terminal symmetric-monopole MTDC system is protected and the converters are fault-tolerant inductor-capacitor-inductor (LCL) VSCs. This type of converters allows limiting the DC current during fault conditions up to the rated current value [91]. The fault-clearing time is around 30–60 ms.

Reference [92] proposes a differential-current algorithm for fault detection and identification on a 4-terminal meshed MTDC system. A time domain differential algorithm is proposed in Ref. [93]. The model used is a 4-terminal symmetric-monopole MTDC grid. It remains stable during all possible external disturbances, so it is inherently selective. Reference [94] presents a 4-terminal full-bridge MMC-HVDC system. This type of converter can actively control DC currents and, this way, the requirement of operation speed is not that critical. Due to this, a differential-current algorithm is chosen as the main protection.

Reference [95] presents a protection strategy with a series of current measuring sensor distributed every 30 km along the links of a 5-terminal MTDC system employing half-bridge MMCs. This way, the measurements taken by two consecutive optical sensors are used to calculate a series of differential-currents, and then they are compared with a threshold. The communication time delay is limited by the distance between adjacent sensors. The differential-current calculation is part of the first of the three stages of the protection strategy. The second stage ensures the fault detection by observing the ROCOC and the last one ensures there is no sensor failure. This strategy enables high speed operation, better stability and reliability.

5.1.4. Directional-current algorithm

The directional-current method is based on detecting if the fault is located in the forward direction, by monitoring the current polarity. A tripping signal is sent to the corresponding CBs when the relays of both ends of the protection zone detect a forward fault [52]. It is a very selective method; however, its operation speed depends on the communication time delay [4].

A directional-current fault detection method is presented in Ref. [96] for a 4-terminal symmetric-monopole VSC-HVDC system. During fault conditions, both currents are flowing from the buses to the link. Another criterion is added to avoid misdetection: current at both link ends must exceed a certain threshold. Authors of [97] propose two alternatives for fault detection: one based on OC and undervoltage algorithms, and the other on ROCOC. In addition, a directional feature is included and the fault current direction is monitored. Protection of a 4-terminal MTDC grid is achieved in Ref. [98] by a directional OC algorithm. Therefore, when an overcurrent is detected, the current direction at the limits of the protection zone is monitored. If the current direction presents opposite directions, the fault is located inside the protection zone.

5.2. Voltage-based protection methods

Protection systems based on algorithms that employ DC voltage signal features are reviewed in the following subsections.

5.2.1. Undervoltage algorithm

A basic voltage-based method is the undervoltage (UV) algorithm. The magnitude of the DC voltage is compared with a pre-defined threshold [4]. This way, the characteristic voltage drop caused by a fault condition can be detected [55]. It is a fast method but lacks selectivity [52].

A basic UV algorithm is proposed in Ref. [99] to protect a 4-terminal symmetric-monopole MTDC grid. A fault is detected when the voltage drops under a pre-defined threshold. HVDC-CBs and limiting inductors with a size of 100 mH are placed at both end of each link, for improving the selectivity. Similarly, authors of [77] apply the UV algorithm to the same system presented in Ref. [99]. However, in this case, three successive samples of the voltage have to drop under a discrimination threshold of 32 kV and the limiting inductors used are 150 mH. Hence, the UV method achieves fault detection in approximately 1 ms but it does not present a proper performance against high-impedance faults.

On the other hand, a combination of the UV and the OC algorithm is presented in Ref. [100] and applied to the same system presented in Ref. [99]. Three consecutive samples of the voltage magnitude lower than a threshold are needed to achieve fault discrimination, as in Ref. [77]. Moreover, the UV and OC algorithms work independently. This way, the protection system detects a fault when one of the two conditions (OC or UV) is fulfilled. Likewise, another UV-OC combination is presented in Ref. [60]. Both OC and UV conditions have to be satisfied in this case in order to achieve fault detection. Once again, the UV condition is constituted by three consecutive samples. In addition, a communication system is implemented for better performance of this method under long transmission distances.

5.2.2. Rate-of-change-of-voltage algorithm

The DC voltage-derivative is calculated in the rate-of-change-of-voltage (ROCOV) algorithm, as shown in (4):

$$ROCOV = \frac{\Delta V}{\Delta t} = \frac{V_2 - V_1}{t_2 - t_1} \tag{4}$$

where the voltage magnitudes at time t_1 and t_2 are represented by V_1 and V_2, respectively; being time t_2 higher than time t_1.

The variation of the ROCOV magnitude between normal operation (ideally, a value of zero) and fault conditions is used as a fault marker [55]. This method presents fast operation since it is based on the almost instantaneous voltage drop produced by a fault condition [4,52]. Moreover, the ROCOV magnitude decreases when fault distance increases [52], so it allows internal and external fault discrimination [101]. Therefore, the voltage-derivative value is compared with a pre-defined threshold in order to achieve fault detection and discrimination [52].

Reference [102] proposes a ROCOV-based main protection for a 9-terminal bipole MTDC system. The rate of change of the DC link voltage is calculated and then it is compared with a certain threshold. This protection system adopts a full-selective fault-clearing strategy placing H-CBs in series with 100 mH limiting inductors at both ends of each link. This way, only the faulty link will be isolated. Similarly, the ROCOV algorithm protects a 4-terminal symmetric-monopole MMC-HVDC grid. The ROCOV is calculated locally and compared with a discrimination threshold of −200 kV/ms. As in the previous reference, H-CBs and limiting inductors with a size of 100 mH are selected, following a full-selective strategy. The ROCOV method presents a detection time lower than 1 ms and it is capable of detecting high-impedance faults up to 750 Ω PtP faults and 400 Ω PtG faults.

Authors of [103] present a ROCOV method for fault detection in a

4-terminal bipole MMC-MTDC system. The operation of this algorithm is challenging against fault conditions with impedances higher than 100 Ω. Thus, authors propose an adaptive threshold value to improve its selectivity against high-impedance faults: a curve fitting method is employed to estimate a fault impedance interval and, then, the adaptive threshold value is obtained, taking into account the maximum ROCOV value for an external fault condition with the estimated impedance.

Reference [101] presents a protection system based on the ROCOV algorithm for 3-terminal bipole VSC-HVDC system with one overhead line and two underground cables. 100 mH inductors delimit the protection zones. The ROCOV is employed as the main link protection and busbar protection. The main protection calculates the ROCOV locally at both ends of the line. However, comparing the magnitude of the ROCOV at both sides of the inductors, an internal bus fault is detected when the voltage-derivative at the bus side of the inductor exceeds the voltage-derivative at the line side. The authors of [104] propose a method to identify the fault direction for improved reliability, sensitivity and speed of the protection method presented in Ref. [101]. Thus, the ROCOV at both sides of the line terminal inductors are compared: if the line side ROCOV is the highest, the fault is located on the protected line; otherwise, it is an external or bus fault. In addition, an undervoltage condition is used as a supervision element. In order to improve the performance against high-impedance faults, a communication channel is added since the speed requirement is not a constraint.

5.2.3. Reactor voltage algorithm

The voltage across the limiting inductors is used as a fault marker in Ref. [105]. If this voltage exceeds a determined threshold, a tripping signal is issued. Similarly, authors of [106] employ the voltage across the DC reactor as a fault marker. Fault type discrimination is achieved by comparing the difference between the reactor voltages of both poles: a PtP fault is identified if this difference is lower than a pre-defined threshold; otherwise, a PtG fault is identified and the faulty pole is the one with the highest absolute reactor voltage. In addition, a communication-based backup protection for high-impedance faults is presented; a fault is detected when the absolute reactor voltage is higher than a threshold, which is lower than the main protection threshold. Then, the amplitude and directional information of the reactor voltages at both ends of the protection zones are used for faulty line and faulty pole identification, respectively. This method was tested through simulations on a 4-terminal VSC-HVDC grid. It operates within 1 μs for low-impedance faults and within 2 ms for high-impedance faults.

Authors of [107] also propose a fault detection algorithm based on the voltage variation across the 200 mH inductors of a meshed 3-terminal symmetric-monopole MMC-HVDC system. The time interval required by the DC voltage across the inductor to exceed two thresholds is used as fault marker. This way, a fault is detected when this time interval is less than a threshold, since the voltage across the inductor increases faster for internal faults.

On the other hand, reference [108] presents a main and backup protection scheme based on the ratio of the transient voltages at both sides of the limiting inductors. During fault conditions, the transient voltage in the line side of the limiting inductor will be higher than the transient voltage in the converter side, increasing the value of the ratio. Hence, a fault is detected when the ratio overcomes a pre-defined threshold value. The main protection only uses local measurements while the backup protection employs a communication system in order to improve the performance of the protection scheme against high-impedance faults. It was analysed on a 5-terminal symmetric-monopole VSC-HVDC grid with 10 mH limiting inductors. Similarly, the authors of [109] also employ measurements at both sides of the limiting inductors. In this case, this alternative is based on comparing the ratio between the ROCOV at both sides of the limiting inductors with a threshold; forward fault detection is achieved when the ratio overcomes the threshold. This implies higher operation speed: fault detection and discrimination are achieved in less than 200 μs.

5.2.4. Sheath voltage algorithm

The sheath voltage is used as fault marker in Ref. [110]. During normal operation, sheath voltage magnitude is zero and no current flows across the cable sheath. However, under fault conditions, fault current flows across the cable sheath and very fast and severe overvoltages are produced. The proposed method can classify faults in PtP, positive PtG, negative PtG, unbalanced positive pole capacitor bank and unbalanced negative pole capacitor bank. The link with the highest sheath voltage is identified as the faulty part of the grid. Then, the sheath voltages of both poles are compared and the highest one indicates the faulty pole. But if both voltages are equal, there is a PtP fault. DC faults and unbalanced capacitors can be distinguished according to the polarity of the sheath voltage peak. In the positive pole, the peak is positive during DC faults and negative during unbalanced capacitor conditions while the opposite happens in the negative pole.

5.3. Traveling-wave-based methods

After fault inception, the current and voltage signals change at the fault point causing a fault wave to propagate rapidly throughout the DC grid [4,8,55]. The most common traveling wave method is based on detecting the initial wave front at its arrival to the relaying points [52], which presents a fast and accurate operation [111,112]. This method can be single-ended or double-ended, depending on the number of ends used to gather information. The signal wave contains useful information for fault detection and location [4]. Then, this interesting information has to be extracted and processed [6]. However, it presents challenges in terms of mathematically modelling the traveling wave, detecting the wave-head, incapability of detecting close-up faults, different traveling wave speed in underground cables and overhead lines (OHL), and need of a high sampling rate [69].

5.3.1. First carrier frequency harmonic current

First Carrier Frequency Harmonic (FCFH) currents are characteristic of pulse-width modulation (PWM) converters. When the system is under a fault condition, this type of converter generates FCFH current, which flows through the DC link capacitors following a round path with a different direction depending on the location and characteristics of the fault condition [113–115]. During internal faults, the relays can detect the FCFH of the DC current since they are located after the DC link capacitors. Meanwhile, when an external fault occurs, this frequency content is not detected since the DC link capacitors filter them. Considering that the FCFH current varies under different fault conditions [116–121], it can be employed as a key feature to detect and identify fault conditions in transmission systems equipped with PWM converters. However, the value of the FCFH current decreases during high-impedance faults, and so does the algorithm's sensitivity [115].

A FCFH current-based algorithm protects a 4-terminal VSC-HVDC system in Ref. [114]. The harmonic content is extracted using the short-time Fourier transform. Two conditions have to be fulfilled for fault detection: the FCFH current and its number of pulses have to exceed their respective thresholds. Similarly, Hilbert-Huang Transform is employed in Ref. [113]. Meanwhile, the high frequency content of the current is extracted using the discrete Fourier transform in Ref. [85]. In this case, the magnitude of the zero-crossing frequency bins (those frequencies where the pre-fault current frequency spectrum periodically crosses zero) in the frequency spectrum is used as fault marker, since it increases during fault conditions due to harmonic distortion. The performance of the method is analysed in two models, both of them based on a 4-terminal symmetric-monopole VSC-HVDC system, but with different configurations: radial and ring. This way, fault detection is achieved in less than 1 ms, but it is not adequate to high-impedance faults and it is vulnerable to noise. In addition, its performance is influenced by the fault location since the frequency magnitude varies with it.

5.3.2. Fourier transform

Fourier Transform is a very relevant signal processing tool and it is used to extract a signal's frequency content, i.e., its frequency-amplitude representation. However, no time information is available in a Fourier-transformed signal. In other words, the Fourier Transform indicates the existence of a frequency component regardless the inception instant of this component [122].

Discrete time Fourier transform is used in Ref. [67] to analyse the frequency spectral pattern of the DC current. Fault detection is achieved by observing the distortion of the frequency due to the high frequency content. Fault detection is achieved in Ref. [66] using the ratio between the standard deviation and the mean value of a certain range of the frequency spectrum obtained by the fast Fourier transform. Regarding fault location, the relationship between the gap between consecutive frequency peaks and the fault distance is used: the closer the fault is to the relay point, the larger the frequency gap is. PtP and PtG faults are discriminated comparing the frequency spectrum of both poles.

5.3.3. Wavelet transform

Wavelet Transform (WT) is based on multiresolution analysis, where the signal is analysed with different resolutions at different frequencies, extracting the frequency information of the traveling wave signal [123]. This way, the high frequency information is obtained with a good time resolution and a poor frequency resolution, while low frequency information is obtained with a poor time resolution and a good frequency resolution [122].

WT is used to extract the energy content of the positive line DC current in Ref. [65]. A decision tree is formed using the energy-coefficients to recognize the fault location and type. The current-wavelet-coefficients are used as input data for a fuzzy voter in Ref. [124] in order to figure out the affected line and the fault type. A fault location algorithm is added to this method in Ref. [125]. It consists of the time difference between the arrivals of the first traveling wave and the first reflected wave. Internal faults are detected in Ref. [64] when the wavelet-coefficient modulus maxima extracted from the DC current presents the same polarity (negative for negative pole and positive for positive pole). The faulty pole is detected comparing the values of the wavelet modulus maxima in both poles. Since similar amplitudes of the forward and backward current traveling waves indicate an internal fault condition, authors of [126] propose using the ratio of the wavelet modulus maxima of these two waves as a fault marker. Internal fault detection is achieved when the ratio is within 0 and 1, and both modulus maxima are higher than a pre-defined threshold. Finally, the fault type is determined comparing the polarities and values of the wavelet modulus maxima at both ends of the link. A backup protection consisting of wavelet packet energy entropy is presented in Ref. [127] against high-impedance PtG faults. Wavelet packet process the current signal and extracts its energy entropy content. Then, the wavelet energy entropy is compared with a threshold, discriminating between internal and external faults. Finally, the fault can be classified using the ratio between the wavelet energy entropies of both poles. H-CBs start their commutation in Ref. [128] when a ROCOC pre-treatment criterion is satisfied. Then, WT extracts the transient energy of the voltages at both sides of the limiting inductors. An internal fault is identified when the difference between both energies exceeds a threshold.

The protection system of [129] employs a stationary, translation-invariant, WT: the fast dyadic wavelet transform in which the calculations are simplified due to sampling the scale parameter along a dyadic sequence. Only local measurements are employed and it is based on three independent criteria: voltage-wavelet-coefficients, current-wavelet-coefficients, and voltage derivative and magnitude. Fault detection is achieved when two out of the three criteria are fulfilled. This redundancy improves the selectivity and reliability. In addition, faulty cable discrimination is achieved by comparing the voltage-wavelet-coefficient amplitudes.

Reference [130] employs a parallel combination of OC and ROCOC algorithms to detect a possible internal fault condition. Afterwards, the WT extracts the frequency content of the current signal. The principal component analysis process the frequency data once again reducing the number of variables but preserving most of the variability of the original data set. Then, a genetic fuzzy systems discriminates between internal and external faults using the data set contributed by the principal component analysis.

5.3.3.1. Continuous wavelet transform. The Continuous Wavelet Transform (CWT) overcomes the time resolution problem associated with the application of the Fourier Transform. This transform is calculated for each frequency component by changing the width of the window. It depends on the translation and scale parameters. The translation parameter indicates the location of the analysis window on the signal and the time information. Meanwhile, the scale parameter indicates the width of the analysis window; a dilated or compressed version of the mother wavelet chosen in order to generate other window functions. However, the computation of the CWT requires a considerable amount of time [122].

Reference [112] uses the CWT to detect and locate fault conditions. Fault detection is achieved when the CWT-coefficient is higher than a certain threshold. These coefficients also indicate the traveling wave arrival times to the terminals. The time difference between both arrivals is used in fault location estimation. Likewise, in Ref. [131] the CWT detects the traveling waves arrival times at both ends of the link in order to locate the fault condition.

5.3.3.2. Discrete wavelet transform. Discrete Wavelet Transform (DWT) is easier to implement than the CWT and presents a reduced computation time. The DWT is based on analysing the signal at different scales by filtering the frequency content. Both high pass and low pass filters are employed. This filtering process affects the resolution. This way, the signal is decomposed by consecutive low pass and high pass filtering into several frequency bands with different resolutions. The outcome of the high pass filter becomes the coefficients of a decomposition level, while the outcome of the low pass filtering is decomposed again through the filtering process. Hence, the higher-level-coefficients, which correspond with low frequency components, present better frequency resolution but worse time resolution than the lower-level-coefficients, which correspond with high frequency components [122].

DWT extracts the high frequency content from the DC current in Refs. [82,132–134]. The wavelet-coefficients are used as fault markers. They are compared with a threshold to detect fault conditions. Conversely [135], uses DWT to process the voltage traveling wave. On the other hand [136], employs the DWT to obtain the high frequency and energy-coefficients from the DC current. If the energy-coefficients exceed a certain threshold and DC currents flows in a positive direction, a fault is detected. Likewise, DWT extracts the current transient high frequency energy in Ref. [137]. Similarly, DWT extracts the energy and high frequency contents of the DC current wave in Ref. [138]. The amplitude of the high frequency transients is used for fast fault detection. The energy-coefficients at both ends of the same pole are similar during normal operation; otherwise, a fault condition is taking place. Then, the energy difference can be used as a fault marker, which is named operating signal. However, a restraining signal is calculated for better selectivity. This signal is the sum of the energy-coefficients at both ends of the same pole. Hence, fault discrimination is achieved by calculating the ratio between the operating and restraining signals; a tripping signal is issued when the operating signal is dominant. Finally, the fault distance is calculated using the arrival time of the traveling waves which are detected when a high frequency peak takes place.

Reference [139] employs the DWT to extract the frequency content of the forward and backward voltage traveling waves. Then, a ratio between the amplitudes of the forward and backward traveling waves is calculated. A forward fault is detected if the ratio is lower than a

pre-defined threshold. Otherwise, a backward fault is detected.

5.3.4. Other traveling-wave-based methods

Reference [140] employs the MTDC grid presented in Ref. [99] to analyse the performance of the UV algorithm for fault detection and a morphological-gradient-based algorithm for fault discrimination. Fault detection is achieved by comparing the voltage drop to a pre-selected threshold value. Then, the fault-induced voltage traveling wave is processed by a morphological gradient technique. This is a non-linear and time-domain method, useful for edge detection, which is applied to extract the fault-induced voltage transients. Thus, fault discrimination is achieved by comparing the morphological gradient amplitudes.

Authors of [141] propose a protection system based on local voltage and current measurements. Fault detection is achieved by analysing the fault transient voltage waveform, which is previously filtered by a fifth-order high-pass Butterworth filter in order to obtain the fault-related high-frequency voltage waveform. Then, the period between the fault-induced abrupt changes (peak and valley) on the voltage waveform, i.e., the first peak time, is calculated. An internal fault is detected when the calculated first peak time is lower than a pre-defined threshold value. In addition, faulty pole discrimination is achieved using the ratio between the current variation of the positive and negative poles.

The DC voltage and current signals are processed by the median absolute deviation in Ref. [142]. This statistical technique is able to robustly locate the abrupt changes of a transient. Then, the processed signals are compared with their respective thresholds and a fault is detected when both criteria are fulfilled.

5.4. Artificial intelligence

Artificial intelligence is a collection of computing concepts, which are able to recognize patterns and to identify highly nonlinear class boundaries in the input data [6]. They try to resemble the behaviour of human beings. Then, artificial intelligence techniques try to automate rational decisions made by a person. This way, they can include missing data, be adaptable to evolving situations and improve their performance progressively based on accumulated experience [69].

The performance of the artificial neural network (ANN) is inspired by the behaviour of the biological neural network [6]. Some characteristics of ANNs are: pattern recognition, generalisation and interpolation within the parameter space, distributed representation and strong learning capability [2]. After a training process, they can distinguish non-linear relationships between input and output data without knowing their internal processes. They can diagnose the system from feature content extracted from the fault signal [143]. ANN-based methods present an accurate, robust and fast performance for fault detection and location [144]. However, the ANN's training stage is designed specifically for each system and it is a time-consuming process [8], but their speed of operation is fast.

Reference [69] proposes an ANN-based transient protection scheme. It detects, locates and classifies faults on the OHLs of a 3-terminal MTDC grid model. Three different ANNs achieve these three fault identification operations, independently. Moreover, it shows fast speed (less than 5 ms), reliability and accuracy in fault detection and location, and an improved robustness to high-impedance and close-up faults. The input data for the three ANNs is the high frequency content from the fault current signal, which is extracted using the discrete Fourier transform, and only the magnitude of the frequencies is used. On the other hand [68], presents a comparison between three different ANN based algorithms for fault detection and location in a 4-terminal VSC-HVDC system. These three algorithms are based on local current measurements. The first algorithm directly uses DC current samples as input data. Meanwhile, in the second one, the discrete Fourier transform processes the DC current to extract its frequency spectrum, which would be the input data of the ANNs. In the case of the third algorithm, the input data is composed by the wavelet-coefficients extracted from the DC current using the DWT. Each line of the grid has two ANNs, for fault location and detection, respectively. From the comparison of the three algorithms, it is concluded that the third one presents better performance and accuracy, since the responses of the other two ones present difficulties during far-end fault scenarios.

6. Comparison

A comparison of the different protection systems found on the literature for MTDC systems is summarised in Table 2, in alphabetical order, according to the protection system used. Firstly, the protection systems are classified considering the grid's characteristics:

- VSC technology: two-level VSC (2L-VSC), three-level VSC (3L-VSC), LCL-VSC, half-bridge MMC (HB-MMC) or full-bridge MMC (FB-MMC).
- System configuration: monopole (MonoP), symmetric-monopole (S-MonoP) or bipole (BiP).
- Line type and length: regarding the use of OHL or cables in the MTDC and their respective lengths.

Then, the different protection systems are classified regarding their characteristics:

- Local-measurement-based algorithm (Loc) or communication-based algorithm (Com).
- Adopted fault-clearing strategy: full-selective, partially-selective or non-selective.
- Breaking device: AC-CB, DC switch, HVDC-CB, H-CB, SS-CB, M − CB or DC/DC converter.
- Size of the limiting inductors located in series with the HVDC-CBs.
- Performance against high-impedance fault.
- Fault detection time: related to the time needed by the algorithm to detect a fault.
- Fault clearing time: includes the algorithm's fault detection time and the breaking device's operation time.

The remaining abbreviations used in Table 2 are: fault detection method (FDet), fault location method (FLoc), fault location time (tloc), fault isolation method (FIso), fault isolation time (tiso), grid partition method (GPar), grid partition time (tgpar), main protection (M), busbar protection (BB), backup protection (BU), differential-current (DiffCurr), discrete time Fourier transform (DTFT), fast Fourier transform (FFT), high-impedance fault condition (HIF), low-impedance fault condition (LIF).

From this comparison, it can be concluded that local-measurement-based algorithms are the most usual ones, instead of communication-based algorithms, due to their faster operation. In addition, current-measurement-based methods are more usually employed compared to voltage-measurement-based methods. It must be highlighted that a considerably high number of protection system employ a combination of several methods. By using each method for different conditions, their advantageous characteristics are combined and the performance of the protection system is improved in terms of selectivity, sensitivity and robustness.

Similarly, the most common converter technology is the half-bridge modular multilevel converter, whilst the most used system configurations are bipole and symmetric-monopole. Likewise, full-selective strategies are predominant, as well as H-CBs, which are chosen rather than SS-CBs and M-CBs. Meanwhile, AC-CBs are selected when non-selective and partially-selective strategies are adopted. In the case of partially-selective strategies, HVDC-CBs are preferred for the grid partition stage, while AC-CBs and DC switches are preferred for the fault isolation stage. Furthermore, the size of the limiting inductors varies mainly in the range of 50 and 150 mH, being the most common value 100 mH.

Table 2
Comparison of the reviewed protection methods.

REF.	YEAR	PROTECTION SYSTEM	LOC/ COM	CONVERTER	CONFIGURATION	LINE TYPE	LINE LENGTH	FAULT CLEARING STRATEGY	BREAKING DEVICE	LIMITING REACTOR	FAULT IMPEDANCE	FAULT DETECTION TIME	FAULT CLEARING TIME
[69]	2017	ANN	Loc	2L-VSC	S-MonoP	OHL	200 km	Full-selective	HVDC-CB	–	100 Ω	4.5 ms; tloc: 26 ms	–
[68]	2018			VSC	MonoP		650, 530, 370 km					<5 ms	
[112]	2012	CWT	Com	VSC	–	OHL	24, 44, 97 km	Full-selective	HVDC-CB	–	–	–	–
[131]	2014					Cable	5, 20, 30, 40, 50, 70 km				100 Ω		
[56]	2012	DiffCurr	Com	VSC	BiP	Cable	25, 50, 75, 100, 200 km	Full-selective	HVDC-CB	40 mH	200 Ω	0.3–1 ms	–
[89]	2014			VSC		OHL	25, 50, 75, 100, 200 km		HVDC-CB	–	10 Ω	–	–
[88]	2013			2L-VSC		Cable	25, 50, 75, 100, 200 km		HVDC-CB	–	500 Ω	–	–
[90]	2013			2L-VSC		Cable	25, 50, 75, 100, 200 km		H-CB	30 mH	200 Ω	–	1–3 ms
[94]	2018			FB-MMC		OHL/ Cable	200, 300, 400, 500 km		M-CB	5 mH	400 Ω	–	20 ms
[92]	2014	DiffCurr	Com	VSC	S-MonoP	Cable	–	Full-selective	–	–	–	–	–
[93]	2015			VSC			100, 150, 200 km		H-CB	–	–	–	–
[87]	2015			LCL-VSC			600 km		HVDC-CB	–	–	–	30–60 ms
[95]	2017			HB-MMC			90, 120, 150, 180, 300 km		H-CB	150 mH	300 Ω	–	3–4 ms
[96]	2015	Directional-current	Com	VSC	S-MonoP	Cable	–	Full-selective	SS/H/M-CB	50–100 mH	7 Ω	–	1/2–5/60 ms
[98]	2015	Directional-current	Com	HB-MMC	S-MonoP	Cable	35.5, 100, 107, 110, 200 km	Non-selective	AC-CB and DC switch	–	7 Ω	–	60 ms
[97]	2013	Directional-current	Loc	2L-VSC	–	Cable	300, 500 km	Full-selective	HVDC-CB	–	–	–	15 ms
[67]	2016	DTFT	Loc	MMC	S-MonoP	OHL and cable	200 km	Full-selective	HVDC-CB	–	–	–	–
[138]	2016	DWT	Com	2L/3L-VSC/ HB-MMC	BiP	OHL and cable	60, 200, 300 km	Full-selective	HVDC-CB	–	300 Ω	–	–
[145]	2017	DWT	Loc	VSC	BiP	OHL and cable	30, 60, 200, 300 km	Full-selective	SS/H CB	–	150 Ω	–	2.2/3.2 ms
[82]	2018			VSC	–	–	–		HVDC-CB	–	–	–	–
[137]	2019			VSC	–	OHL	100, 200, 300 km		HVDC-CB	100 mH	300 Ω	1 ms	–
[134]	2016			2L-VSC	–	Cable	–		H-CB	10 mH	–	–	–
[133]	2017			MMC	MonoP	–	100, 200 km		HVDC-CB	–	500 Ω	1 ms	–
[136]	2016			HB-MMC	BiP	Cable	200, 300, 400 km		HVDC-CB	–	–	1 ms	–
[139]	2020			MMC	–	OHL	542, 908 km		–	50, 150, 500 mH	–	–	–
[135]	2018	DWT (M) DiffCurr (BB)	Loc	MMC	S-MonoP	OHL	100, 120, 150, 180, 200, 300, 600 km	Full-selective	H-CB	150 mH	500 Ω	1 ms	–

(*continued on next page*)

Table 2 (*continued*)

REF.	YEAR	PROTECTION SYSTEM	LOC/ COM	CONVERTER	CONFIGURATION	LINE TYPE	LINE LENGTH	FAULT CLEARING STRATEGY	BREAKING DEVICE	LIMITING REACTOR	FAULT IMPEDANCE	FAULT DETECTION TIME	FAULT CLEARING TIME
[85]	2018	FCFH	Loc	VSC	S-MonoP	Cable	200 km	Full-selective	HVDC-CB	100 mH	10 Ω	<1 ms	–
[114]	2018			2L-VSC			–			–	50 Ω	–	–
[113]	2019			2L/3L-VSC			–			–	500 Ω	–	–
[66]	2018	FFT	Loc (FDet) Com (FLoc)	VSC	–	Cable	170, 200, 360, 460 km	Full-selective	HVDC-CB	–	Solid	1 ms tloc: 10 ms	–
[73]	2014	OC	Com	VSC	–	–	–	Partially-selective	H-CB and DC switch	–	100 Ω	–	5 ms (H-CB) tiso: 70 ms (DC switch)
[70]	2010	OC	Loc	VSC	–	Cable	–	Full-selective	HVDC-CB	–	–	–	–
[58]	2015			HB-MMC	BiP		200, 300 km		–	10, 100, 500 mH	–	–	2–3 ms
[72]	2017			HB-MMC	–		–		H-CB	8 mH	–	–	5 ms
[77]	2019			HB-MMC	S-MonoP		100, 150, 200 km		H-CB	150 mH	200 Ω PtP 20 Ω PtG	1–5 ms	3–7 ms
[74]	2015	OC	Loc	HB-MMC	–	Cable	50, 80, 100 km	Partially-selective	GPar: HVDC-CB FIso: AC-CB	100 mH	–	–	tgpar: 12–13 ms tiso: 63–65 ms
[75]	2016						50, 80, 100 km		GPar: HVDC-CB or DC/DC conv. FIso: AC-CB and DC switch			–	tgpar: 7–9 ms (HVDC-CB)/3–6 ms (DC/DC conv.) tiso: 83–87 ms
[76]	2016						50, 75, 80, 100, 120 km		GPar: DC/DC converter FIso: AC-CB and DC switch or M-CB			–	tgpar: 4–8 ms tiso: 104–108 (AC-CB)/24–28 ms (M – CB)
[71]	2016	OC (M) DiffCurr (BB)	Loc (M) Loc/ Com (BB)	HB-MMC	S-MonoP	Cable	100, 150, 200 km	Full-selective	HVDC-CB	100 mH	Solid	–	–
[78]	2018	OC-UV-ROCOC combination	Loc	HB-MMC	BiP	OHL	50, 320, 330, 450 km	Full-selective	SS-CB	Not employed	20 Ω	–	8.74–11.26 ms
[130]	2018	OC-ROCOC-WT combination	Loc	2L-VSC	S-MonoP	Cable	200 km	Full-selective	HVDC-CB	–	10 Ω	1.4 ms	–
[105]	2014	Reactor Voltage	Loc	2L-VSC	BiP	Cable	25, 50, 75, 100, 200 km	Full-selective	HVDC-CB	10, 15, 20, 25, 30, 35, 40, 45 mH	50 Ω	–	1–2 ms
[107]	2017			MMC	S-MonoP	OHL and cable	100, 150 km			200 mH	1000 Ω	1–4 ms	–
[106]	2018			HB-MMC	S-MonoP/BiP	Cable	100, 200 km			150 mH	380 Ω	1 μs (LIF) 2 ms (HIF)	–
[108]	2017	Reactor Voltage	Loc (M) Com (BU)	VSC	S-MonoP	OHL and cable	70, 100, 200 km	Full-selective	HVDC-CB	10 mH	200 Ω	0.2–0.9 ms	–
[86]	2018	ROC of DiffCurr	Com	MMC	–	–	60, 120 km	Full-selective	HVDC-CB	–	–	–	–
[61]	2014	ROCOC	Com	2L-VSC	–	Cable	170, 200, 360, 400 km	Full-selective	HVDC-CB	–	Solid	–	2–9 ms
[84]	2012	ROCOC	Loc	VSC	–	Cable	–	Full-selective	HVDC-CB	–	–	–	–
[82]	2018			VSC	–	–	–		HVDC-CB	–	–	–	–
[80]	2015			MMC	BiP	Cable	150, 400 km		HVDC-CB	10 mH	Solid	–	3 ms

(*continued on next page*)

Table 2 (*continued*)

REF.	YEAR	PROTECTION SYSTEM	LOC/ COM	CONVERTER	CONFIGURATION	LINE TYPE	LINE LENGTH	FAULT CLEARING STRATEGY	BREAKING DEVICE	LIMITING REACTOR	FAULT IMPEDANCE	FAULT DETECTION TIME	FAULT CLEARING TIME
[81]	2019			HB-MMC	BiP	OHL and cable	100,500, 1500 km		HVDC-CB	40 mH	50 Ω	1 ms	–
[77]	2019			HB-MMC	S-MonoP	Cable	100, 150, 250 km		H-CB	100 mH	5 Ω PtP 2 Ω PtG	0.095–1.25 ms	2.095–3.25 ms
[83]	2016	ROCOC (M) DiffCurr (BU)	Loc (M) Com (BU)	MMC	BiP	Cable	150, 400 km	Full-selective	HVDC-CB	25 mH	75 Ω (M) 400 Ω (BU)	–	2–3 ms (M) 13 ms (BU)
[85]	2018	ROCOC correlation-coefficient	Loc	VSC	S-MonoP	Cable	200 km	Full-selective	HVDC-CB	100 mH	10 Ω	–	1 ms
[101]	2016	ROCOV	Loc	MMC	BiP	OHL and cable	100, 500, 1500 km	Full-selective	H-CB	100 mH	–	–	3 ms
[109]	2018			MMC	BiP	OHL and cable	100, 500, 1100, 1500 km			40 mH	200 Ω	200 μs	–
[77]	2019			HB-MMC	S-MonoP	Cable	100, 150, 200 km			100 mH	750 Ω PtP 400 Ω PtG	0.005–1.1 ms	2.005–3.1 ms
[103]	2020			MMC	BiP	OHL	500 km			200 mH	300 Ω	1 ms	–
[102]	2015	ROCOV (M) OC (HIF)	Loc	MMC	BiP	OHL and cable	100, 200, 300, 400, 500 km	Full-selective	H-CB	100 mH	10 Ω	–	3 ms
[104]	2017	ROCOV (M) ROCOV-UV (HIF)	Loc (M) Com (HIF)	MMC	BiP	OHL and cable	100, 500, 1500 km	Full-selective	H-CB	50, 100, 125 mH	200 Ω	–	3 ms
[110]	2017	Sheath Voltage	Loc	2L-VSC	BiP	Cable	60, 80, 100 km	–	–	–	100 Ω	5 ms	–
[140]	2019	Traveling wave	Loc	HB-MMC	S-MonoP	Cable	100, 150, 200 km	Full-selective	HVDC-CB	50 mH	200 Ω	1 ms	–
[141]	2019			HB-MMC	BiP	OHL	50, 188, 206, 208 km		HVDC-CB	200 mH	400 Ω	1 ms	–
[142]	2020			LCL-VSC	–	Cable	200 km		M-CB	20 mH	Solid	2 ms	10 ms
[99]	2015	UV	Loc	HB-MMC	S-MonoP	Cable	100, 150, 200 km	Full-selective	H-CB	100 mH 150 mH	– 15 Ω PtP 5 Ω PtG	3–4 ms 0.205–1.375 ms	5–6 ms 2.205–3.375 ms
[77]	2019												
[60]	2019	UV-OC combination	Com Loc	HB-MMC	S-MonoP	Cable	100, 150, 200 km	Full-selective	H-CB	100 mH	Solid	4–5 ms 0.35–3.35 ms	6–7 ms 2.35–5.35 ms
[100]													
[64]	2018	WT	Com	2L-VSC	BiP	OHL	100, 120, 150 km	Full-selective	HVDC-CB	–	400 Ω	–	3 ms
[126]	2018			2L-VSC	BiP	Cable	80, 100, 150, 200 km			–	400 Ω	–	–
[127]	2019			MMC	S-MonoP	OHL	50, 100, 150, 200 km			100 mH	1000 Ω	–	–
[129]	2011	WT	Loc	VSC	BiP	Cable	400 km	Full-selective	HVDC-CB	–	Solid	1 ms	–
[128]	2018	WT (M) DiffCurr (BU)	Loc (M) Com (BU)	VSC	–	Cable	6, 8, 10 km	Full-selective	H-CB	–	50 Ω	–	2–4 ms

To sum things up, it can be concluded that the tendency is to use a combination of protection algorithms for improved reliability, preferably local-measurement-based algorithms due to speed and operation constraints in transmission distances of hundreds of kilometres. In addition, full-selective fault-clearing strategies, along with H-CBs, may have great relevance in future projects, as, e.g., in the Zhangbei MTDC project in China [47].

7. Conclusions

This paper reviews different protection systems found on the literature, specifically applied to VSC-MTDC grids. Moreover, the problematic fault features and behaviour on a VSC-based system are presented. In addition, the protection devices that can be implemented in a HVDC system are described, as well as fault-clearing strategies. The performance requirements that have to be fulfilled by the protection method are also explained.

The classification of protection methods regarding how the measurements are taken is highlighted. Communication-based algorithms are highly selective, however, they are restricted by both the communication time delay and the correct operation of the communication channel. Meanwhile, local-measurement-based algorithms present high operation speed, but their selectivity is challenging. They need the application of limiting inductors in order to delimit the protection zones and improve their selectivity. These components reduce the fast increase of the current during fault conditions, then, circuit breakers with lower current interruption capability can be implemented, in spite of a higher energy dissipation capability.

The protection algorithms reviewed are: current-based methods (overcurrent, ROCOC, differential-current and directional-current), voltage-based methods (undervoltage, ROCOV, reactor and sheath voltages), traveling-wave-based methods (FCFH current, Wavelet and Fourier transforms) and artificial intelligence methods. The main characteristics and features of these protection systems are summarised and compared.

It can be concluded that the actual tendency of MTDC protection systems employs predominantly local-current-measurement-based algorithms, as well as H-CBs, full-selective strategy and half-bridge MMCs. Moreover, the preferred system configuration varies between bipole and symmetric-monopole. Similarly, the most selected size of the limiting inductors is 100 mH. In addition, a combination of different protection methods can benefit the performance of the protection system.

Declaration of competing interest

The authors declare that they have no known competing financial interests or personal relationships that could have appeared to influence the work reported in this paper.

Acknowledgement

The authors gratefully acknowledge the support from the Spanish Ministry of Economy, Industry and Competitiveness (project ENE2016-79145-R AEI/FEDER, UE), the Basque Government (GISEL research group IT1191-19) and the University of the Basque Country UPV/EHU (GISEL research group 181/18).

References

[1] CIGRÉ WG B4.52. HVDC grid feasibility study. Cigré; 2013. Available: https://e-cigre.org/publication/533-hvdc-grid-feasibility-study. [Accessed 19 December 2019].
[2] Ramesh M, Laxmi AJ. Fault identification in HVDC using artificial intelligence — recent trends and perspective. In: International conference on power, signals, controls and computation; 2012. Thrissur, Kerala, India, 3-6 January 2012.
[3] Peng T, Tzelepis D, Dysko A, Glesk I. Assessment of fault location techniques in voltage source converter based HVDC systems. In: IEEE Texas power and energy conference (TPEC); 2017. College Station, TX, USA, 9-10 February 2017.
[4] Psaras V, Emhemed A, Adam G, Burt GM. Review and evaluation of the state of the art of DC fault detection for HVDC grids. In: 53rd international universities power engineering conference (UPEC); 2018. Glasgow, Scotland, 4-7 September 2018.
[5] Li B, He J, Li Y, Li B. A review of the protection for the multi-terminal VSC-HVDC grid. Protect Contr Mod Power Syst 2019;4(1):21.
[6] Le Blond S, Bertho R, Coury DV, Vieira JCM. Design of protection schemes for multi-terminal HVDC systems. Renew Sustain Energy Rev 2016;56:965–74.
[7] Zhang L, Zou Y, Yu J, Qin J, Vittal V, Karady GG, Shi D, Wang Z. Modeling, control, and protection of modular multilevel converter-based multi-terminal HVDC systems: a review. CSEE J Power Energy Syst 2017;3(4):340–52.
[8] Farhadi M, Mohammed OA. Protection of multi-terminal and distributed DC systems: design challenges and techniques. Elec Power Syst Res 2017;143:715–27.
[9] Oñederra O, Odriozola H, Planas E, Lopez I, López V. Overview of DC technology. Energy conversion. Renew Energy Power Qual J 2013;11:630–5.
[10] Kulkarni S, Santoso S. Interrupting short-circuit direct current using an AC circuit breaker in series with a reactor. Adv Power Electron 2012:805958. 2012.
[11] Jovcic D, van Hertem D, Linden K, Taisne J, Grieshaber W. Feasibility of DC transmission networks. In: 2nd IEEE PES international conference and exhibition on innovative smart grid technologies, Manchester, UK; 2011. p. 1–8. 5-7 December 2011.
[12] Mokhberdoran A, Carvalho A, Leite H, Silva N. A review on HVDC circuit breakers. In: 3rd renewable power generation conference (RPG 2014), Naples, Italy; 2014. p. 1–6. 24-25 September.
[13] Hajian M, Jovcic D, Wu B. Evaluation of semiconductor based methods for fault isolation on high voltage DC grids. IEEE Trans Smart Grid 2013;4(2):1171–9.
[14] Baran ME, Mahajan NR. Overcurrent protection on voltage-source-converter-based multiterminal DC distribution systems. IEEE Trans Power Deliv 2007;22(1):406–12.
[15] Leterme W, Van Hertem D. Classification of fault clearing strategies for HVDC grids. In: CIGRÉ Lund symposium, Lund, Sweden; May 2015. p. 27–8.
[16] Larruskain DM, Abarrategui O, Zamora I, Buigues G, Valverde V, Iturregi A. Requirements for fault protection in HVDC grids. Renew Energy Power Qual J 2015;13:322–6.
[17] Taherbaneh M, Jovcic D, Taisne JP, Nguefeu S. DC fault performance and cost analysis of DC grids for connecting multiple offshore wind farms. In: IEEE Grenoble conference, Grenoble, France; 2013. p. 1–6. 16-20 June 2013.
[18] Bucher MK, Franck CM. fault current interruption in multiterminal HVDC networks. IEEE Trans Power Deliv 2016;31(1):87–95.
[19] Franck CM. HVDC circuit breakers: a review identifying future research needs. IEEE Trans Power Deliv 2011;26(2):998–1007.
[20] Abedrabbo M, Leterme W, Van Hertem D. Systematic approach to HVDC circuit breaker sizing. IEEE Trans Power Deliv 2020;35(1):288–300.
[21] Yang S. Feasibility and simulation study of DC hybrid circuit breakers. Toronto, Canada: Master of Applied Science Thesis, University of Toronto; 2014.
[22] Sander R, Leibfried T. Considerations on energy absorption of HVDC circuit breakers. In: 49th international universities power engineering conference (UPEC); 2014. p. 1–6. Cluj-Napoca, Romania, 2-5 September.
[23] Gawande AG, Wasankar MK. Hybrid HVDC breaker. Int J Innovat Res Dev 2014;3(1):119–22.
[24] Ekström A, Härtel H, Lips HP, Schultz W, Joss P, Holfeld H, Kind D. Design and testing of an HVDC circuit-breaker. In: International conference on large HIgh voltage electric systems. Paris: France; 1976. 25 August - 2 September.
[25] Liu S, Popov M. Development of HVDC system-level mechanical circuit breaker model. Int J Electr Power Energy Syst 2018;103:159–67.
[26] Qu L, Yu Z, Xiao X, Zhao W, Huang Y, Zeng R. Development and application of a 10 kV mechanical DC circuit breaker. Energies 2019;12(19).
[27] Greenwood AN, Barkan P, Kracht WC. HYDC vacuum circuit breakers. IEEE Trans Power Apparatus Syst 1972;PAS-91(4):1575–88.
[28] Shan Y, Lim TC, Williams BW, Finney SJ. Successful fault current interruption on DC circuit breaker. IET Power Electron 2016;9(2):207–18.
[29] Magnusson J. On the design of hybrid DC-breakers consisting of a mechanical switch and semiconducor devices. Stockholm, Sweden: Licenciate Thesis, Kungliga Tekniska Högskolan; 2015.
[30] Davidson CC, Whitehouse RS, Barker CD, Dupraz J, Grieshaber W. A new ultra-fast HVDC circuit breaker for meshed DC networks. In: 11th IET international conference on AC and DC power transmission, Birmingham, UK; 2015. p. 1–7. 10-12 Feb.
[31] Finney S. "DC faults", EES-UETP 2014 HVDC technology and applications. 2014. Glasgow, Scotland, 1-5 December.
[32] Premerlani WJ. Forced commutation performance of vacuum switches for HVDC breaker application. IEEE Power Eng Rev 1982;PER-2(8):46.
[33] Eriksson T, Backman M, Halen S. A low loss mechanical HVDC breaker for HVDC grid applications. In: Cigré 2014. Paris: France; August 2014. p. 25–9.
[34] Andersson D, Henriksson A. Passive and active DC breakers in the three gorges-changzhou HVDC project. In: CIGRE international conference on power systems (ICPS2001), Wuhan, China; 2001. p. 391–5. 3-5 September.
[35] Du C, Wang C. Review of DC circuit breaker technology for HVDC application. In: 22nd international conference on electrical machines and systems (ICEMS), Harbin, China; 2019. p. 1–6. 11-14 August.
[36] Ängquist L, Nee S, Modeer T, Baudoin A, Norrga S, Belda NA. Design and test of VSC assisted resonant current (VARC) DC circuit breaker. In: 15th IET international conference on AC and DC power transmission (ACDC 2019), coventry, UK; 2019. p. 1–6. 5-7 February.

[37] Liu S, Popov M, Mirhosseini SS, Nee S, Modeer T, Ängquist L, Belda N, Koreman K, van der Meijden, Mart AMM. Modeling, experimental validation, and application of VARC HVDC circuit breakers. IEEE Trans Power Deliv 2020;35(3): 1515–26.
[38] Mokhberdoran A, Carvalho A, Silva N, Leite H, Carrapatoso A. A new topology of fast solid-state HVDC circuit breaker for offshore wind integration applications. In: 17th European conference on power electronics and applications (EPE'15 ECCE-europe), Geneva, Switzerland; 2015. p. 1–10. 8-10 September.
[39] Kempkes M, Roth I, Gaudreau M. Solid-state circuit breakers for medium voltage DC power. In: IEEE electric ship technologies symposium, Alexandria, VA, USA; 2011. p. 254–7. 10-13 April 2011.
[40] Meyer C, Kowal M, De Doncker RW. Circuit breaker concepts for future high-power DC-applications. In: Fourtieth IAS annual meeting. Conference record of the 2005 Industry applications conference, Kowloon, Hong Kong, China; 2005. p. 860–6. 2-6 October.
[41] Xiang W, Hua Y, Wen J, Yao M, Li N. Research on fast solid state DC breaker based on a natural current zero-crossing point. J Mod Power Syst Clean Energy 2014;2(1):30–8.
[42] Lin W, Jovcic D, Nguefeu S, Saad H. Modelling of high-power hybrid DC circuit breaker for grid-level studies. IET Power Electron 2016;9(2):237–46.
[43] Derakhshanfar R, Jonsson TU, Steiger U, Habert M. Hybrid HVDC breaker - technology and applications in point-to-point connections and DC grids. In: 2014 cigre session, Paris, France; 2014. 24-29 August.
[44] Kim BC, Chung Y, Hwang HD, Mok HS. Development of HVDC circuit breaker with fast interruption speed. In: 9th international conference on power electronics and ECCE Asia (ICPE-ECCE Asia); 2015. p. 2844–8. Seoul, South Korea, 1-5 June.
[45] Geebelen B, Leterme W, Van Hertem D. Analysis of DC breaker requirements for different HVDC grid protection schemes. In: 11th IET international conference on AC and DC power transmission; 2015. p. 1–7. Birmingham, UK, 10-12 February.
[46] Häfner J, Jacobson B. Proactive hybrid HVDC breakers - a key innovation for reliable HVDC grids. In: The electric power system of the future - integrating supergrids and microgrids international symposium; 2011. Bologna, Italy, 13-15 September.
[47] Jovcic D, Tang G, Pang H. Adopting circuit breakers for high-voltage dc networks: appropriating the vast advantages of dc transmission grids. IEEE Power Energy Mag 2019;17(3):82–93.
[48] Zhou J, Li H, Xie R, Liu L, Nie W, Song K, Huo F, Liang D. Research of DC circuit breaker applied on zhoushan multi-terminal VSC-HVDC project. In: IEEE PES Asia-Pacific power and energy engineering conference (APPEEC). China: Xi'an; 2016. p. 1636–40. 25-28 October.
[49] Tang G, Pang H, He Z, Wei X. Research on key technology and equipment for zhangbei 500kV DC grid. In: International power electronics conference (IPEC-Niigata 2018 -ECCE Asia). Niigata, Japan; 2018. p. 2343–51. 20-24 May 2018.
[50] Leterme W, Jahn I, Ruffing P, Sharifabadi K, Van Hertem D. Designing for high-voltage dc grid protection: fault clearing strategies and protection algorithms. IEEE Power Energy Mag 2019;17(3):73–81.
[51] Pérez-Molina MJ, Larruskain DM, Eguía López P, Buigues G. Challenges for protection of future HVDC grids. Front Energy Res 2020;8.
[52] Jahn I, Johannesson N, Norrga S. Survey of methods for selective DC fault detection in MTDC grids. In: 13th IET international conference on AC and DC power transmission. Manchester, UK: ACDC 2017; 2017. p. 1–7. 14-16 February.
[53] Buigues G, Valverde V, Zamora I, Larruskain DM, Abarrategui O, Iturregi A. DC fault detection in VSC-based HVDC grids used for the integration of renewable energies. In: International conference on clean electrical power (ICCEP), taormina, Italy; 2015. p. 666–73. 16-18 June 2015.
[54] Marten AK, Troitzsch C, Westermann D. Non-telecommunication based DC line fault detection methodology for meshed HVDC grids. IET Gener, Transm Distrib 2016;10(16). 4321-4239.
[55] Li R, Xu L. Review of DC fault protection for HVDC grids. WIREs Energy Environ 2018;7(2).
[56] Descloux J, Rault P, Nguefeu S, Curis J, Guillaud X, Colas F, Raison B. HVDC meshed grid: control and protection of a multi-terminal HVDC system. In: CIGRÉ session Paris. Paris: France; 2012. p. 10. 26-31 August.
[57] Liu Z, Mirhosseini SS, Popov M, Audichya Y, Colangelo D, Jamali S, Palensky P, Hu W, Chen Z. Protection testing for multiterminal high-voltage dc grid: procedures and procedures and assessment. IEEE Ind Electron Mag 2020;14(3): 46–64.
[58] Torres-Olguin RE, Høidalen HK. Inverse time overcurrent protection scheme for fault location in multi-terminal HVDC. In: IEEE eindhoven PowerTech, eindhoven, Netherlands; 2015. 29 June-2 July 2015.
[59] Pérez-Molina MJ, Eguia P, Larruskain DM, Buigues G, Torres E. Non-unit ROCOV scheme for protection of multi-terminal HVDC systems. In: 22nd European conference on power electronics and applications (EPE ECCE europe 2020); 2020. Lyon, France, 7-11 September.
[60] Pérez-Molina MJ, Larruskain DM, Eguia Lopez P, Abarrategi O, Santos-Mugica M. A comparison of non-unit and unit protection algorithms for HVDC grids. In: AEIT HVDC international conference 2019; 2019. Florence, Italy, 9-10 May.
[61] Dallas I, Booth C. Teleprotection in multi-terminal HVDC supergrids. In: 12th IET international conference on developments in power system protection (DPSP 2014); 2014. p. 1–6. Copenhagen, Denmark, 31 March-3 April.
[62] Leterme W, Beerten J, Van Hertem D. Nonunit protection of HVDC grids with inductive DC cable termination. IEEE Trans Power Deliv 2016;31(2):820–8.
[63] Naidoo D, Ijumba NM. HVDC line protection for the proposed future HVDC systems. In: International conference on power system technology, vol. 2. Singapore, Singapore: PowerCon 2004; 2004. p. 1327–32. 21-24 November 2004.
[64] Zou G, Feng Q, Huang Q, Sun C, Gao H. A fast protection scheme for VSC based multi-terminal DC grid. Int J Electr Power Energy Syst 2018;98:307–14.
[65] Mallick RK, Patnaik RK. Fault analysis of voltage-source converter based multi-terminal HVDC transmission links. In: International conference on energy, automation and signal; 2011. p. 1–7. Bhubaneswar, Odisha, India, 28-30 Dec. 2011.
[66] Li J, Yang Q, Mu H, Le Blond S, Hongwen h. A new fault detection and fault location method for multi-terminal high voltage direct current of offshore wind farm. Appl Energy 2018;220:13–20.
[67] Yeap YM, Ukil A, Geddada N. STFT analysis of high frequency components in transient signals in multi-terminal HVDC system. In: Iecon 2016 - 42nd annual conference of the IEEE industrial electronics society; 2016. p. 4008–13. Florence, Italy, 23-26 October.
[68] Torres J, Santos R, Asano P. A comparison of new methods based on ANNs for detecting and locating faults in MTDC systems. In: International conference on smart energy systems and technologies. Sevilla, Spain: SEST); 2018. p. 1–6. 10-12 September 2018.
[69] Yang Q, Le Blond S, Aggarwal R, Wang Y, Li J. New ANN method for multi-terminal HVDC protection relaying. Elec Power Syst Res 2017;148:192–201.
[70] Yang J, Fletcher JE, O'Reilly J, Adam GP, Fan S. Protection scheme design for meshed VSC-HVDC transmission systems of large-scale wind farms. In: 9th IET international conference on AC and DC power transmission. London, UK: ACDC 2010); 2010. 19-21 October.
[71] Mokhberdoran A, Silva N, Leite H, Carvalho A. Unidirectional protection strategy for multi-terminal HVDC grids. Trans Environ Electr Eng 2016;1(4).
[72] Wang Y, Yuan Z, Fu J, Li Y, Zhao Y. A feasible coordination protection strategy for MMC-MTDC systems under DC faults. Int J Electr Power Energy Syst 2017;90: 103–11.
[73] Monadi M, Koch-Ciobotaru C, Luna A, Candela JI, Rodriguez P. A protection strategy for fault detection and location for multi-terminal MVDC distribution systems with renewable energy systems. In: International conference on renewable energy research and application. Milwaukee, WI, USA: ICRERA); 2014. p. 496–501. 19-22 October 2014.
[74] Rahman H, Xu L, Bell K. DC fault protection of multi-terminal HVDC systems using DC network partition and DC circuit breakers. In: Protection, automation and control world conference. Glasgow, UK: PAC World 2015; 2015. 29 June - 2 July.
[75] Rahman MH, Xu L, Yao Liangzhong. DC fault protection strategy considering DC network partition. In: IEEE power and energy society general meeting (PESGM); 2016. p. 1–5. Boston, MA, USA, 17-21 July.
[76] Rahman MH, Xu L, Yao L. Protection of large partitioned MTDC Networks Using DC-DC converters and circuit breakers. Protect Contr Mod Power Syst 2016;1(1): 19.
[77] Pérez Molina MJ, Larruskain DM, Eguía López P, Etxegarai A. Analysis of local measurement-based algorithms for fault detection in a multi-terminal HVDC grid. Energies 2019;12(24).
[78] Stumpe M, Tünnerhoff P, Dave J, Schnettler A, Ergin D, Schön A, Würflinger K, Schettler F. DC fault protection for modular multi-level converter-based HVDC multi-terminal systems with solid state circuit breakers. IET Gener Transm Distrib 2018;12(12):3013–20. https://doi.org/10.1049/iet-gtd.2017.1322. Available:.
[79] Ikhide MA, Tennakoon SB, Griffiths A, Subramanian S, Ha H, Adamczyk A. Limitations of di/dt technique in DC line protection. In: 13th international conference on development in power system protection 2016 (DPSP); 2016. Edinburgh, UK, 7-10 March.
[80] Marvik JI, D'Arco S, Sharifabadi K. Protection scheme for multi-terminal radial VSC HVDC system without communication between terminals. In: CIGRÉ Lund symposium; 2015. Lund, Sweden, 27-28 May.
[81] Haleem MN, Rajapakse AD. fault type discrimination in HVDC transmission lines using rate of change of local currents. IEEE Trans Power Deliv 2020;35(1): 117–29.
[82] Geddada N, Yeap YM, Ukil A. Experimental validation of fault identification in VSC-based DC grid system. IEEE Trans Ind Electron 2018;65(6):4799–809.
[83] Marvik JI, D'Arco S, Suul JA. A two-layer detection strategy for protecting multi-terminal HVDC systems against faults within a wide range of impedances. In: 13th international conference on development in power system protection 2016. Edinburgh, UK: DPSP; 2016. p. 1–6. 7-10 March.
[84] Fletcher SDA, Norman PJ, Galloway S, Burt G. Fault detection and location in DC systems from initial di/dt measurement. In: Euro tech con conference; 2012. Manchester, UK.
[85] Yeap YM, Geddada N, Satpathi K, Ukil A. Time- and frequency-domain fault detection in a VSC-interfaced experimental DC test system. IEEE Trans Ind Inf 2018;14(10):4353–64.
[86] Ota R, Kinjo R, Matayoshi H, Senjyu T, Howlader AM. DC fault detection method using current differential deviation in MTDC grid. In: IEEE PES Asia-Pacific power and energy engineering conference. Kota Kinabalu, Malaysia: APPEEC); 2018. p. 139–42. 7-10 October 2018.
[87] Hajian M, Zhang L, Jovcic D. DC transmission grid with low-speed protection using mechanical DC circuit breakers. IEEE Trans Power Deliv 2015;30(3): 1383–91.
[88] Descloux J, Gandioli C, Raison B, Hadjsaid N, Tixador P. Protection system for meshed HVDC network using superconducting fault current limiters. In: IEEE Grenoble conference; 2013. Grenoble, France, 16-20 June 2013.
[89] Razzaghi R, Paolone M, Rachidi F, Descloux J, Raison B, Retière N. Fault location in multi-terminal HVDC networks based on electromagnetic time reversal with limited time reversal window. In: Power systems computation conference, Wroclaw, Poland; 2014. 18-22 August 2014.

[90] Descloux J, Raison B, Curis J. Protection strategy for undersea MTDC grids. In: IEEE Grenoble conference; 2013. Grenoble, France, 16-20 June 2013.
[91] Jovcic D, Zhang L, Hajian M. LCL VSC converter for high-power applications. IEEE Trans Power Deliv 2013;28(1):137–44.
[92] Adamczyk A, Barker CD, Ha H. Fault detection and branch identification for HVDC grids. In: 12th IET international conference on developments in power system protection. DPSP 2014); 2014. Copenhagen, Denmark, 31 March-3 April.
[93] Johannesson N, Norrga S. Longitudinal differential protection based on the universal line model. In: Iecon 2015 - 41st annual conference of the IEEE industrial electronics society; 2015. p. 1091. Yokohama, Japan, 9-12 November.
[94] Jovcic D, Lin W, Nguefeu S, Saad H. Low-energy protection system for DC grids based on full-bridge MMC converters. IEEE Trans Power Deliv 2018;33(4): 1934–43.
[95] Tzelepis D, Dyśko A, Fusiek G, Nelson J, Niewczas P, Vozikis D, Orr P, Gordon N, Booth C. Single-ended differential protection in MTDC networks using optical sensors. IEEE Trans Power Deliv 2017;32:1605–15.
[96] Kontos E, Pinto RT, Rodrigues S, Bauer P. Impact of HVDC transmission system topology on multiterminal DC network faults. IEEE Trans Power Deliv 2015;30 (2):844–52.
[97] Marvik JI, Svendsen HG. Analysis of grid faults in offshore wind farm with HVDC connection. Energy Procedia 2013;35:81–90.
[98] Kontos E, Pinto RT, Bauer P. Fast DC fault recovery technique for H-bridge MMC-based HVDC networks. In: IEEE energy conversion congress and exposition (ECCE); 2015. p. 3351–8. Montreal, QC, Canada, 20-24 Sept. 2015.
[99] Leterme W, Ahmed N, Beerten J, Ängquist L, Hertem DV, Norrga S. A new HVDC grid test system for HVDC grid dynamics and protection studies in EMT-type software. In: 11th IET international conference on AC and DC power transmission; 2015. Birmingham, UK, 10-12 February.
[100] Pérez-Molina MJ, Eguía-Lopez P, Larruskain DM, Santos Mugica M, Rodriguez-Sanchez R. Evaluation of a local fault detection algorithm for HVDC systems. Renew Energy Power Qual J 2019;17:262–7.
[101] Sneath J, Rajapakse AD. fault detection and interruption in an earthed HVDC grid using ROCOV and hybrid DC breakers. IEEE Trans Power Deliv 2016;31(3): 973–81.
[102] Sneath J, Rajapakse AD. DC fault protection of a nine-terminal MMC HVDC grid. In: 11th IET international conference on AC and DC power transmission; 2015. p. 1–8. Birmingham, UK, 10-12 February.
[103] Zhang C, Song G, Wang T, Dong X. An improved non-unit traveling wave protection method with adaptive threshold value and its application in HVDC grids. IEEE Trans Power Deliv 2020;35(4):1800–11.
[104] Haleem NM, Rajapakse AD. Application of new directional logic to improve DC side fault discrimination for high resistance faults in HVDC grids. J Mod Power Syst Clean Energy 2017;5(4):560–73.
[105] Descloux J, Raison B, Curis J. Protection algorithm based on differential voltage measurement for MTDC grids. In: 12th IET international conference on developments in power system protection. Copenhagen, Denmark: DPSP 2014); 2014. 31 March-3 April.
[106] Li C, Gole AM, Zhao C. A fast DC fault detection method using DC reactor voltages in HVdc grids. IEEE Trans Power Deliv 2018;33(5):2254–64.
[107] Li R, Xu L, Yao L. DC fault detection and location in meshed multiterminal HVDC systems based on DC reactor voltage change rate. IEEE Trans Power Deliv 2017; 32(3):1516–26.
[108] Liu J, Tai N, Fan C. Transient-voltage-based protection scheme for DC line faults in the multiterminal VSC-HVDC system. IEEE Trans Power Deliv 2017;32(3): 1483–94.
[109] Haleem NM, Rajapakse AD. Local measurement based ultra-fast directional ROCOV scheme for protecting Bi-pole HVDC grids with a metallic return conductor. Int J Electr Power Energy Syst 2018;98:323–30.
[110] Ashrafi Niaki SH, Hosseini SM, Abdoos AA. Fault detection of HVDC cable in multi-terminal offshore wind farms using transient sheath voltage. IET Renew Power Gener 2017;11(13):1707–13.
[111] Azazi S, Sanaye-Pasand M, Abedini M, Hasani A. A traveling-wave-based methodology for wide-area fault location in multiterminal DC systems. IEEE Trans Power Deliv 2014;29(6):2552–60.
[112] Nanayakkara OMKK, Rajapakse AD, Wachal R. Traveling-wave-based line fault location in star-connected multiterminal HVDC systems. IEEE Trans Power Deliv 2012;27(4):2286–94.
[113] Ashouri M, Faria dS, Bak CL. A harmonic based pilot protection scheme for VSC-MTDC grids with PWM converters. Energies 2019;12(10):1010.
[114] Ashouri M, Khazraj H, da Silva FF, Leth Bak C. Protection of multi-terminal VSC-HVDC grids based on the response of the first carrier frequency harmonic current. In: 53rd international universities power engineering conference. Glasgow, UK: UPEC); 2018. p. 1–5. 4-7 September 2018.
[115] Zheng X, Tai N, Wu Z, Thorp J. Harmonic current protection scheme for voltage source converter-based high-voltage direct current transmission system. IET Gener, Transm Distrib 2014;8(9):1509–15.
[116] Holmes DG, McGrath BP. Opportunities for harmonic cancellation with carrier-based PWM for a two-level and multilevel cascaded inverters. IEEE Trans Ind Appl 2001;37(2):574–82.
[117] Holmes G, Lipo T, Lipo TA. Pulse width modulation for power converters: principles and practice. first ed. Hoboken, NJ, USA: John Wiley & Sons; 2003.
[118] Bierhoff M, Fuchs FW. DC link harmonics of three phase voltage source converters influenced by the pulse width modulation strategy-an analysis. In: 31st annual conference of IEEE industrial electronics society. Raleigh, NC, USA: IECON 2005.; 2005. p. 6. 6-10 November 2005.
[119] Flourentzou N, Agelidis VG, Demetriades GD. VSC-based HVDC power transmission systems: an overview. IEEE Trans Power Electron 2009;24(3): 592–602.
[120] McGrath BP, Holmes DG. A general analytical method for calculating inverter DC-link current harmonics. IEEE Trans Ind Appl 2009;45(5):1851–9.
[121] Odavic M, Sumner M, Zanchetta P, Clare JC. A theoretical analysis of the harmonic content of PWM waveforms for multiple-frequency modulators. IEEE Trans Power Electron 2010;25(1):131–41.
[122] Polikar R. The wavelet tutorial - the engineer's ultimate guide to wavelet analysis. second ed. Glassboro, NJ, USA: Rowan University; 2001.
[123] Shang L, Liang W. The review of high voltage DC transmission lines fault location. Int J Comput Commun Contr 2014;3(4):21–8.
[124] Eldin AH, Lotfy A, Elgamal M, Ebeed M. Protection oriented observability in multi-terminal HVDC systems. In: 7th international conference on information and communication systems (ICICS), irbid, Jordan, 5-7 april 2016; 2016. p. 102–8.
[125] Hossam-Eldin A, Lotfy A, Elgamal M, Ebeed M. Combined traveling wave and fuzzy logic based fault location in multi-terminal HVDC systems. In: IEEE 16th international conference on environment and electrical engineering (EEEIC); 2016. p. 1–6. Florence, Italy, 7-10 June.
[126] Jiang L, Chen Q, Huang W, Wang L, Zeng Y, Zhao P. Pilot protection based on amplitude of directional travelling wave for voltage source converter-high voltage direct current (VSC-HVDC) transmission lines. Energies 2018;11(8).
[127] Huai Q, Liu K, Qin L, Liao X, Zhu S, Li Y, Ding H. Backup-protection scheme for multi-terminal HVDC system based on wavelet-packet-energy entropy. IEEE Access 2019;7:49790–803.
[128] Luo Yiping, He Jinghan, Luo Guomin, Zhang Yongjie. Fast DC fault location and isolation strategy for the flexible multi-terminal DC system. J Eng 2018;(15): 908–12.
[129] Kerf KD, Srivastava K, Reza M, Bekaert D, Cole S, Hertem DV, Belmans R. Wavelet-based protection strategy for DC faults in multi-terminal VSC HVDC systems. IET Gener, Transm Distrib 2011;5(4):496–503.
[130] Bertho R, Lacerda VA, Monaro RM, Vieira JCM, Coury DV. Selective nonunit protection technique for multiterminal VSC-HVDC grids. IEEE Trans Power Deliv 2018;33(5):2106–14.
[131] Azizi S, Afsharnia S, Sanaye-Pasand M. Fault location on multi-terminal DC systems using synchronized current measurements. Int J Electr Power Energy Syst 2014;63:779–86.
[132] Saleem U, Arshad U, Masood B, Gul T, Khan WA, Ellahi M. Faults detection and classification of HVDC transmission lines of using discrete wavelet transform. In: International conference on engineering and emerging technologies. Lahore, Pakistan: ICEET); 2018. p. 1–6. 22-23 February 2018.
[133] Yeap YM, Geddada N, Ukil A. Analysis and validation of wavelet transform based DC fault detection in HVDC system. Appl Soft Comput 2017;61:17–29.
[134] Mitra B, Chowdhury B, Manjrekar M. Fault analysis and hybrid protection scheme for multi-terminal HVDC using wavelet transform. In: North American power symposium (NAPS); 2016. p. 1–6. Denver, CO, USA, 18-20 September 2016.
[135] Tzelepis D, Dyśko A, Blair SM, Rousis AO, Mirsaeidi S, Booth C, Dong X. Centralised busbar differential and wavelet-based line protection system for multi-terminal direct current grids, with practical IEC-61869-compliant measurements. IET Gener, Transm Distrib 2018;12(14):3578–86.
[136] Torres-Olguin RE, Hoidalen HK. Travelling waves-based fault detection method in multi-terminal HVDC grids connecting offshore wind farms. In: 13th international conference on development in power system protection 2016. Edinburgh, UK: DPSP); 2016. 7-10 March.
[137] Li Y, Wu L, Li J, Xiong L, Zhang X, Song G, Xu Z. DC fault detection in MTDC systems based on transient high frequency of current. IEEE Trans Power Deliv 2019;34(3):950–62.
[138] Abu-Elanien AEB, Elserougi AA, Abdel-Khalik AS, Massoud AM, Ahmed S. A differential protection technique for multi-terminal HVDC. Elec Power Syst Res 2016;130:78–88.
[139] Li B, Li Y, He J, Li B, Liu S, Liu B, Xu L. An improved transient traveling-wave based direction criterion for multi-terminal HVDC grid. IEEE Trans Power Deliv 2020;35(5):2517–29.
[140] Jamali S, Sattar Mirhosseini S. Protection of transmission lines in multi-terminal HVDC grids using travelling waves morphological gradient. Int J Electr Power Energy Syst 2019;108:125–34.
[141] Huang Q, Zou G, Wei X, Sun C, Gao H. A non-unit line protection scheme for MMC-based multi-terminal HVDC grid. Int J Electr Power Energy Syst 2019;107: 1–9. Available, http://www.sciencedirect.com/science/article/pii/S0142061518314996.
[142] Liu L, Liu Z, Popov M, Palensky P, Van Der Meijdenm M. A fast protection of multi-terminal HVDC system based on transient signal detection. IEEE Trans Power Deliv 2020;1.
[143] Sun X, Tong X, Yin J. Fault diagnosis for VSC-HVDC using wavelet transform. In: Asia-pacific power and energy engineering conference; 2012. Shanghai, China, 27-29 March 2012.
[144] Mirzaei M, Kadir Z, Moazami E, Hizam H. Review of fault location methods for distribution power system. Aust J Basic Appl Sci 2009;3:2670–6.
[145] Abu Elanien A, Abdel-Khalik A, Massoud A, Ahmed S. A non-communication based protection algorithm for multi-terminal HVDC grids. Elec Power Syst Res 2017;144:41–51.